ORNL/TM-6805

Interim Report on the ORNL Absolute Measurements of $\bar{\nu}_p$ for ^{252}Cf

R. R. Spencer
R. Gwin
R. Ingle
H. Weaver

OAK RIDGE NATIONAL LABORATORY
OPERATED BY UNION CARBIDE CORPORATION · FOR THE DEPARTMENT OF ENERGY

ORNL/TM-6805
ENDF-285

Contract No. W-7405-eng-26

Engineering Physics Division

INTERIM REPORT ON THE ORNL ABSOLUTE MEASUREMENTS OF $\bar{\nu}_p$ FOR ^{252}Cf

R. R. Spencer, R. Gwin, R. Ingle,† and H. Weaver

Manuscript Completed - June 29, 1979
Date Published - September 1979

†Instrumentation and Controls Division

NOTICE This document contains information of preliminary nature. It is subject to revision or correction and therefore does not represent a final report.

Prepared by the
OAK RIDGE NATIONAL LABORATORY
Oak Ridge, Tennessee 37830
operated by
UNION CARBIDE CORPORATION
for the
DEPARTMENT OF ENERGY

CONTENTS

BLANK PAGE

ABSTRACT

An initial effort has been made to measure absolutely the average number of prompt neutrons, $\bar{\nu}_p$, emitted in spontaneous fission of ^{252}Cf to an unprecedented accuracy of ± 0.25%. Fission neutrons were counted with a large, gadolinium poisoned, liquid scintillator. A "white source" of neutrons from the ORELA was used to calibrate the detector efficiency as a function of neutron energy. Source neutrons were scattered into the large scintillator by a thin NE-213 proton-recoil detector which employed pulse shape discrimination to eliminate unwanted γ-ray background. The resulting neutron-energy and scattering angle-dependent efficiencies were used to normalize a Monte Carlo calculation of the scintillator efficiency for fission neutrons. Under the assumptions that the effects of parasitic charged particle reactions and multiple neutron scattering in the proton-recoil counter have negligible influence on the efficiency calibration, the value of the average number of prompt neutrons emitted per ^{252}Cf fission was found to be 3.783 ± 0.010. This report is intended as a documentary and guide for future measurements incorporating improvements suggested by the analysis of this first determination.

I. INTRODUCTION

Precise, absolute measurements of the average number of neutrons, $\bar{\nu}$, emitted in the spontaneous fission of ^{252}Cf have been carried out in three different ways in the past: the liquid scintillator method,[1-3] the boron pile method,[4] and the manganese bath method.[5-7] All three require moderation of the fission spectrum neutrons for detection. However, the first two techniques make use of delayed coincidence counting of the neutrons following individual fission events, thus removing the necessity for absolute counting of the fission source rate, whereas the manganese bath requires absolute counting of both the 2.6 hr manganese activity of the solution and the source fission rate. Another important difference is that the coincidence counting is carried out on a sufficiently short time interval following a fission that the effect of delayed neutrons is rendered negligible, whereas the manganese bath method determines the total nubar (prompt plus delayed). In order to compare results of the different experiments use is made of the relation:

$$\bar{\nu}_{total} = \bar{\nu}_{p} + \bar{\nu}_{delayed}$$

where $\bar{\nu}_{delayed}$ is taken to be 0.009 ± 0.004 for ^{252}Cf.[8] Another important difference in the experiments occurs with regard to the emission of delayed gamma rays in fission. Since the liquid scintillator method detects neutrons by means of the capture gamma rays following absorption in the cadmium or gadolinium "poison" of the scintillator solution, a small ($\sim$ 0.3%) correction must be made for sensitivity of the system to a few known, short-lived, gamma emitting isomers formed in fission. To date

this correction has not been directly measurable with the nubar detection system. Rather, it is calculated from previously measured yields, half-lives and gamma ray cascade energies of the isomers coupled to measurements of the scintillator sensitivity to calibrated sources. he boron pile makes use of proportional counter response to the $^{10}B(n,\alpha)$ reaction for neutron detection and like the activation method is not sensitive to delayed gamma rays. This difference cannot be taken lightly due to the relatively good agreement in the reported boron pile and manganese bath results for $\bar{\nu}$ of ^{252}Cf.

Historically, the measurements have consistently shown a systematic discrepancy between the liquid scintillator results on the one hand and the boron pile plus manganese bath results on the other. The boron pile value with a quoted uncertainty of 0.4% was originally 2% lower than the two earliest liquid scintillator values[1,2] which quoted 1% uncertainty each. The boron pile value was reinforced by two manganese bath measurements with uncertainties of 0.5%[5] and 0.4%.[6] The recent addition of another manganese bath value[7] and a more precise liquid scintillator measurement[3] (0.4% uncertainty) along with adjustment of all measurements to account for some small, previously unrecognized sources of error have reduced the discrepancy to 0.7–1.0%. Boldeman[9] and Smith[10] have presented the two most current re-evaluations of all the ^{252}Cf $\bar{\nu}$ measurements. These evaluations include the recent Monte Carlo re-analysis of manganese bath leakage and the boron pile and liquid scintillator neutron detection efficiencies of Ullo and Goldsmith.[11-13] At this point it seems clear that the discrepancy in the previous measurements will not be reduced sufficiently to derive an absolute $\bar{\nu}_p$ of ^{252}Cf to the $\leq$ 0.25% accuracy needed for reactor physics applications.

The importance of such a precise value to both fast breeder and thermal reactor systems stems from the use of californium spontaneous fission sources as a standard in measurements of $\bar{\nu}_p(E_n)$, the neutron energy dependence of nubar, for the fissile isotopes of uranium and plutonium. Experimentally it is convenient to measure the energy dependent nubar ratio

$$R(E_n) = \frac{\bar{\nu}_p(E_n)}{\bar{\nu}_p(^{252}Cf)}$$

for each isotope, thereby avoiding a separate measurement of neutron detector efficiency with each experiment. For a reactor the quantities of interest are the neutron-spectrum-averaged values of $\bar{\nu}$ for each of the heavy metals in the core. Uncertainties in the ratio measurements and in the value of Cf $\bar{\nu}$ contribute directly to uncertainties in the flux-averaged quantities and therefore affect reactor design and cost. For example, sensitivity calculations of a full-scale model LMFBR core[14] indicate that the effect of ν uncertainty is comparable to the more universally recognized sensitivities to σ_f of ^{239}Pu and σ_γ of ^{238}U. It can be seen from Table I of ref. 14 that a 0.5% uncertainty in ^{252}Cf $\bar{\nu}$, since it acts in concert on the $\bar{\nu}$ values of all fissionable isotopes through their measured $R(E_n)$'s, results (to first order) in an uncertainty of 0.5% in multiplication factor, k, and a 1% uncertainty in the so-called k-reset breeding ratio. To meet design goals of 0.5% uncertainty in k and 2% in breeding ratio (only $\sim$ 1/2 of which can be taken up by the nuclear parameters) requires that the ^{252}Cf $\bar{\nu}$ uncertainty be 0.25% or less. Similar conclusions have been reached in the case of light water reactors (LWR).

Recent calculations by Ryskamp[15] predict that the largest effects on LWR fuel-cycle costs were due to ^{252}Cf $\bar{\nu}$ with a sensitivity of approximately 4, compared to typical spectrum averaged cross-section sensitivities of about 0.5. However, the importance of $\bar{\nu}$ for thermal systems is diluted through use of direct measurements with thermal neutrons of the related quantity, η, the number of neutrons emitted per neutron absorbed.

Experiments to determine the average value of the number of neutrons emitted promptly following spontaneous fission of ^{252}Cf have been initiated in part to complement ratio measurements of the energy dependence of $\bar{\nu}$ for the fissile isotopes. Since a number of small corrections necessary in the ratio measurements depend on properties of the particular apparatus used (for example corrections for pulse pile-up and delayed gamma rays), it is desirable to carry out both ratio and absolute measurements, and with the same experimental arrangement as nearly as possible. The primary goal of the present measurement of ^{252}Cf $\bar{\nu}_p$ is to establish a lasting standard for this important constant. To accomplish this the measurement must:

1. attain a higher accuracy than has previously been reported; the optimistic goal of ± 0.25% uncertainty has been adopted;
2. either have eliminated or verified experimentally the known errors and necessary corrections;
3. be sufficiently documented that any necessary future adjustment can be performed expeditiously.

Although the ORNL measurement is being carried out by a well established technique, that is, using a large scintillator tank neutron detector similar to that of previous experimenters,[1-3] there are a number of differences in detail which are felt to be improvements:

1. The neutron efficiency calibration of the tank is carried out over a continuous range of energies with better precision by use of the "white" neutron source from the ORELA.
2. The efficiency calibration, ^{252}Cf measurement and background determinations are obtained simultaneously.
3. The measurement is carried out under extremely low background conditions.
4. Both random and beam-weighted backgrounds are measured.
5. Graphite plugs are used in the tank through-tube to reduce the effect of leakage out the hole.
6. Excellent tank neutron detection stability -- for nine separate runs taken over a period of 24 days the average deviation from the mean of the observed ^{252}Cf $\bar{\nu}$ was 0.028% and the maximum spread in values (highest to lowest value) was 0.079%. The statistical uncertainty of each individual run was $\sim$ 0.02%.

In the first full-blown attempt to measure $\bar{\nu}_p$ of ^{252}Cf at the ORELA facility an apparent uncertainty of 0.26% was attained. This experiment and some important conclusions are reported here.

II. A BRIEF DESCRIPTION OF THE EXPERIMENT

In the ORNL measurement an $\sim$ 900 liter gadolinium loaded liquid scintillator tank was placed in the FP-5 neutron beam from ORELA approximately 85 m from the neutron-producing target. The tank was carefully aligned so that a 1/2" diameter collimated beam traversed the scintillator on the axis of a horizontal through-tube built into the tank. An NE-213 proton recoil detector and a fission chamber containing ^{252}Cf were both positioned on the vertical center axis of the scintillator, the recoil

detector being in the beam and normal to it whereas the fission chamber was out of the beam and just above the through-tube bottom. A schematic of the experimental configuration is given in Fig. 1. Fission events were signalled by coincidence between fragment pulses in the fission detector and the prompt tank pulses from fission gamma rays to allow use of a low fission chamber bias without interference from alpha pulses. When biased well above the alphas, the loss due to the coincidence requirement was only ~ 0.7%. Neutrons scattered from the beam in the NE-213 were signalled by their associated proton recoil pulse. Some 500 ns after either type of event a fast scaler was gated on for 50 μs to record subsequent tank pulses from neutrons slowed down and captured in the scintillator. The nubar scaler data were stored[16] in a Systems Engineering Laboratories (SEL) computer according to the number of pulses counted during this 50 μsec and according to the type of initiating event. From the observed neutron number distributions were obtained: Simultaneously, nubar scaler was triggered by appropriate background pulses and subsequent tank background pulses were recorded. Since only one neutron enters the tank per proton-recoil event, the fraction of recoil events which resulted in a scintillator tank pulse during the 50 μsec counting interval is (after correction for background) a measure of the tank efficiency. These recoil data were used to normalize a Monte Carlo calculation of the total tank efficiency for an isotropic spectrum of neutrons representative of ^{252}Cf fission. This efficiency, together with the background corrected fission event data, permitted the derivation of $\bar{\nu}_p$ for ^{252}Cf.

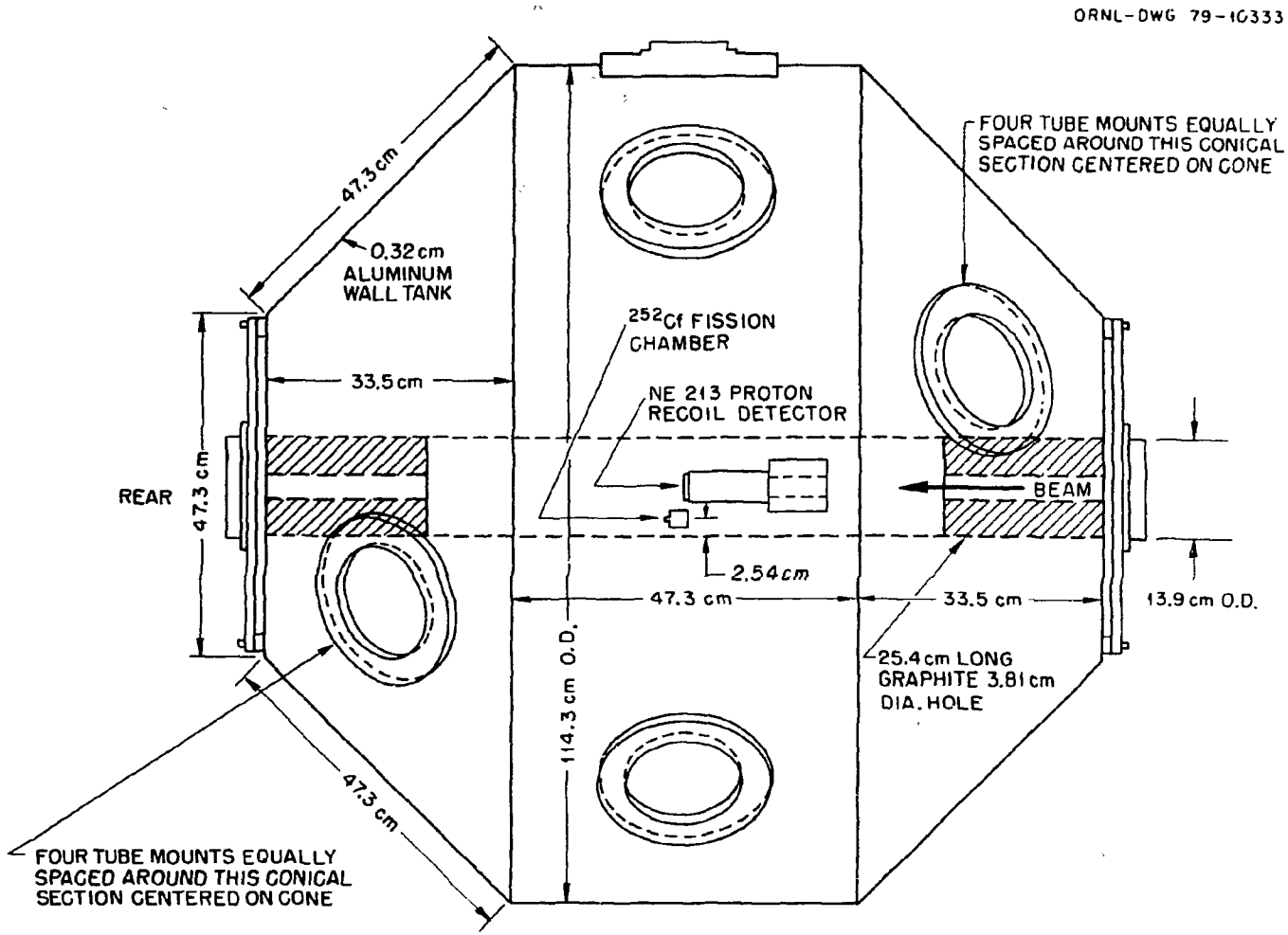

Fig. 1. Schematic cross-section view of the ORNL, gadolinium-loaded scintillator tank with the ^{252}Cf fission chamber and the NE-213 proton-recoil counter in place.

III. THE DETECTOR SYSTEMS

The ^{252}Cf Fission Chamber

Fission fragments from ^{252}Cf were detected in a low mass (22.5 g) ion chamber which was constructed by the Instrument and Controls Division at ORNL.[17] A schematic of the chamber is shown in Fig. 2. Approximately 0.0004 μg of californium (~190 fission/sec) was deposited in a 0.5 cm diameter spot on 0.0127 cm thick nickel foil and overcoated with a thin (24 $\mu g/cm^2$) layer of gold.[18] This source was then spot welded to the inside bottom of the stainless steel outer shell. The chamber was cleaned by high vacuum techniques and filled to 1 atm with pure methane gas. An operating potential of +300 volts was applied to the central electrode with the outer shell grounded. The plate spacing of the chamber was approximately 0.32 cm. An August 29, 1975, mass spectrographic analysis of the californium bulk material from which the source originated is given below:

Isotope	Atomic%
249	11.43
250	20.32
251	7.59
252	60.67

At the time of the present $\bar{\nu}$ measurement (May and June, 1977), it is calculated that approximately 0.2% of the observed source fission rate would be due to the ^{250}Cf contaminant. Assuming $\bar{\nu}$ = 3.50 for this isotope,[19] spontaneous fission of the ^{250}Cf results in a negligible effect (<0.015%) on the present determination of ^{252}Cf $\bar{\nu}$.

ORNL-DWG 79-10334

(1) STAINLESS STEEL CAN
(2) STAINLESS STEEL END PLATE
(3) SMA CONNECTOR (CERAMASEAL; INC)
(4) NICKEL ELECTRODE

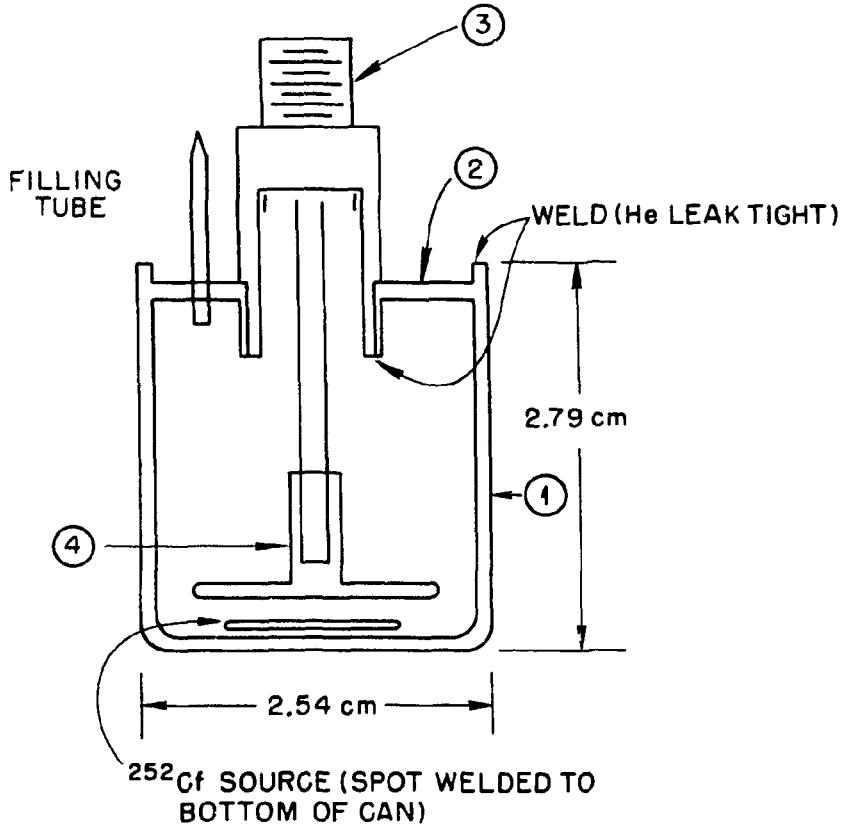

Fig. 2. Schematic cross-sectional view of the ^{252}Cf fission chamber no. 7.

Electronics used with this chamber (see Fig. 13) consisted of an ORTEC 125 FET preamplifier feeding an ORTEC 454 fast amplifier which was coupled to an ORTEC 473 constant fraction discriminator to develop the fast timing signal. The fast amplifier was operated with 20 nsec integration and differentiation time constants. A parallel preamplifier output was used with an ORTEC 472 spectroscopy amplifier to obtain signals for pulse height analysis. Figure 3 shows a typical pulse height spectrum of the fission chamber gated with the fast discriminator output. Good separation between fission pulses and noise-plus-alpha pulses was obtained with relatively few degraded fission pulses in the valley.

The Fission Neutron Detector

Neutrons were detected with an $\sim$ 900 liter tank filled with a pseudo-cumene based liquid scintillator (Nuclear Enterprises NE-224) to which was added gadolinium 2-ethylhexoate to give a concentration of 0.22% by weight natural gadolinium. The tank was constructed from a cylindrical center section and two truncated conical end sections all of 0.3175 cm thick aluminum. Built into this shell was a horizontal through-tube of 6061-T6 aluminum with 13.69 cm I.D. and 0.124 cm wall thickness. The scintillator was viewed by 12 symmetrically arranged RCA 4522 5-inch photomultipliers operated at -2100 v. A photograph of the completed scintillator tank in the experimental position is shown in Fig. 4. Surrounding the detector on four sides and the top was a 25.4 cm thick wall of marble which served to reduce background radiation from ^{40}K in the concrete walls of the bunker. Plan and elevation views of the tank and shielding are shown in Fig. 5.

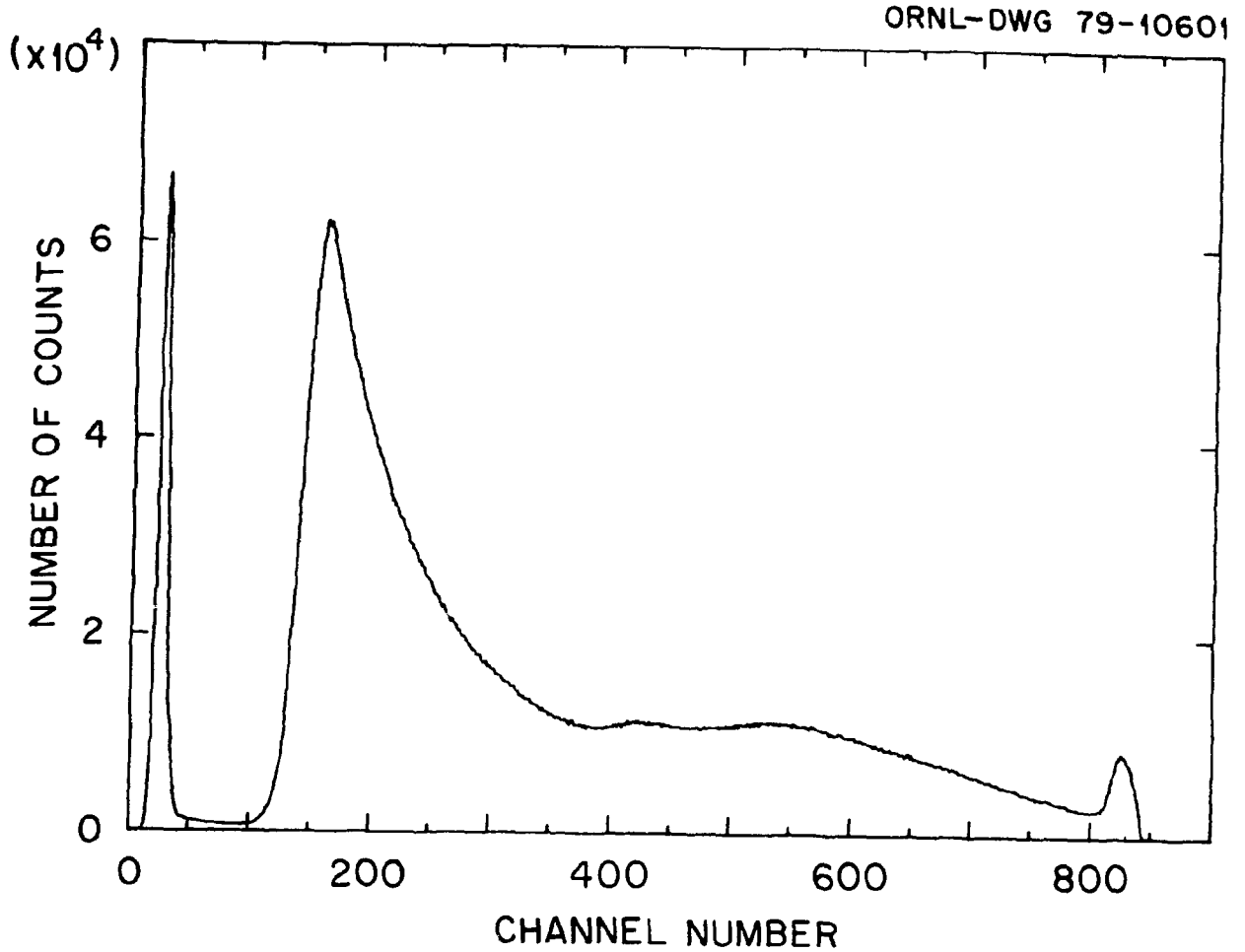

Fig. 3. Gated pulse height spectrum of fission events and alphas + noise from ^{252}Cf chamber no. 7 at + 300 volts and a typical discriminator setting. Channel zero corresponds to zero pulse height. The peak near channel 800 is caused by saturation of the linear amplifier.

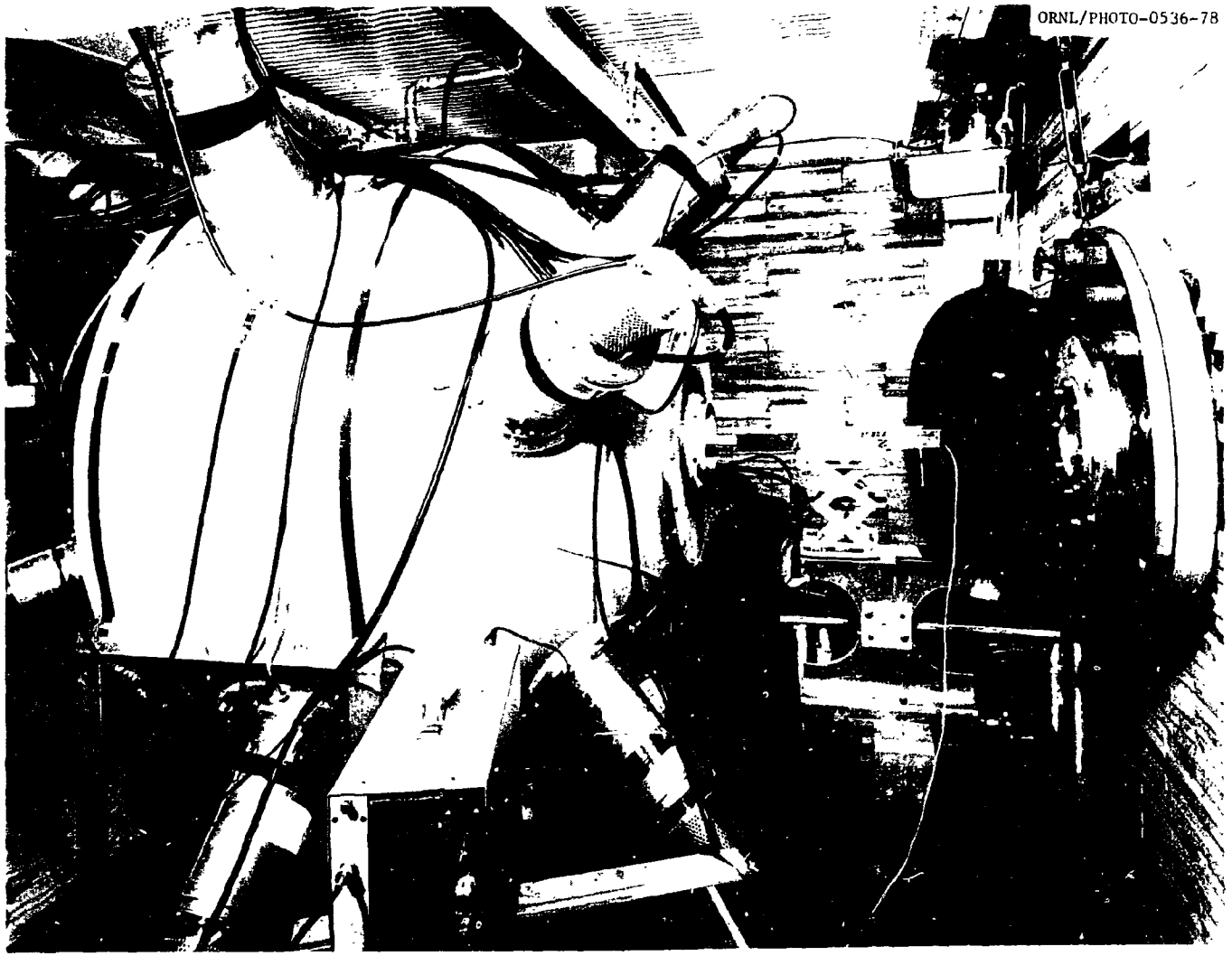

Fig. 4. Picture of the liquid scintillator tank in experimental position inside the marble shielding.

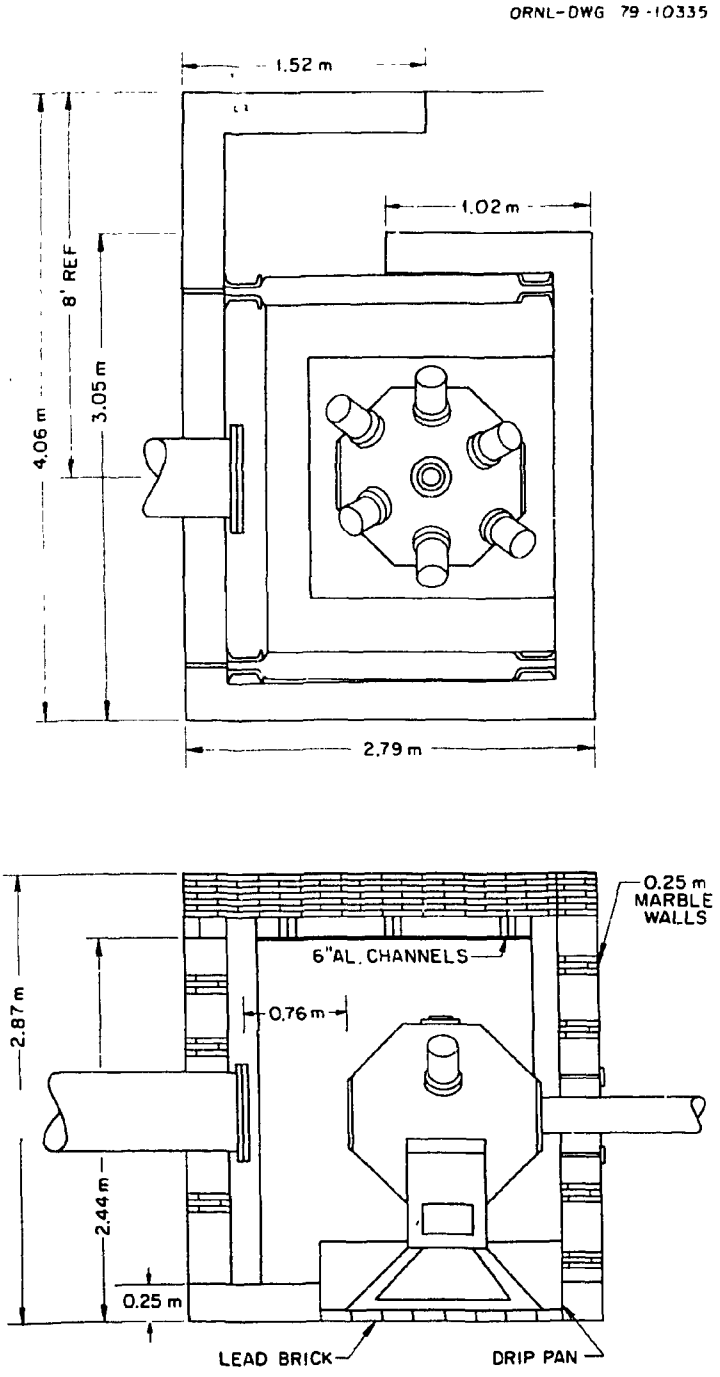

Fig. 5. Plan and elevation views of the experimental facility.

Development of the photomultiplier anode (fast) signals followed conventional techniques. With the help of the ^{252}Cf source, the twelve anode signals were individually matched in pulse height and aligned in time at the output of a summing unit. Pulse height adjustments were made via small changes in high voltage, whereas timing adjustments required addition of appropriate lengths of 50 ohm cable at the input to the summing unit. A constant fraction discriminator (ORTEC 473) was used at the summed output to provide fast logic pulses above a preset pulse height ($\sim$ 930 keV equivalent gamma-ray energy) for presentation to an EG&G T-105 fast trigger (see Fig. 13). The deadtime of the T-105 was set to 100 nsec (nonextending) by means of an external delay cable. This is somewhat longer than the observed natural deadtime ($\sim$ 60 nsec) of the system. The logic output of the T-105 was used to feed the 100 MHz nubar scaler to record neutrons. Prompt coincidence between the tank fast pulses from fission gamma rays and fission chamber pulses was used to select an initiating fission event. The time resolution between the fission chamber and tank fast response to prompt fission gamma rays was measured to be $\leq$ 3.5 nsec FWHM and < 40 nsec FW 1/1000 M. It was, therefore, possible to use a 40 nsec coincidence requirement between the two detectors with negligible loss of fission events.

A slow signal from the scintillator tank was also produced primarily for the purpose of monitoring the system gain and threshold during the experiment. Signals from the photomultiplier 10^{th} dynodes were paralleled into a TC-145 nonblocking preamplifier which fed a TC-200 main amplifier. The main amplifier output was used to study the tank pulse height response to radiations from a variety of sources. Figure 6 shows spectra from sources of ^{137}Cs, ^{65}Zn, ^{22}Na, ^{54}Mn, and ^{60}Co, which were positioned

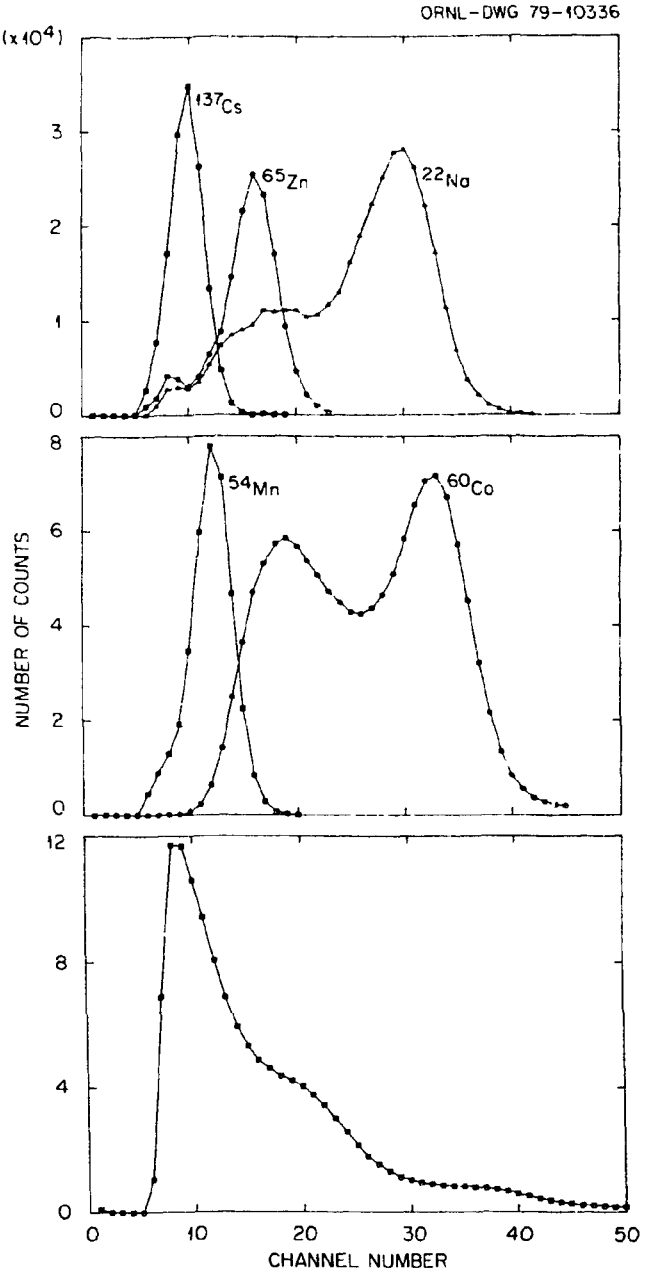

Fig. 6. Scintillator tank pulse height spectra (10th dynode slow pulse output system) of radioactive sources. Top: ^{137}Cs, ^{65}Zn, and ^{22}Na, background subtracted. Middle: background subtracted ^{54}Mn spectrum (ungated) and a ^{60}Co spectrum gated at the $\sim$ 930 keV tank fast pulse discrimination level (background not subtracted). Bottom: typical background spectrum in the tank. ^{40}K natural radiation is visible near channel 20.

at the center of the scintillator tank, and in the lower part of the figure the tank background. Figure 7 shows the tank pulse-height response to ^{252}Cf neutrons (i.e. gated 4 μsec after a fission event) and in the lower portion the response to fission gamma rays (i.e. gated promptly on a fission event). The ^{60}Co, neutron absorption, and ^{252}Cf fission gamma-ray spectra were monitored periodically during the course of the experiment and their positions were observed to be stable to within $\sim$ 1%.

The horizontal through-tube of the tank represents a deviation from spherical symmetry which can cause small, yet significant, errors if anisotropic effects are present in the tank response either to fission neutrons or to scattered calibration neutrons. One possible effect results if the fission fragment detector lacks full 2π efficiency. Thus, the strong correlation in fragment and fission neutron direction could conceivably give an excess (or deficiency) of neutrons traveling in the direction of the hole. Multiple scattering of calibration neutrons in the proton-recoil material could give a similar error in the tank efficiency calibration. Since such asymmetries are difficult to handle computationally, an attempt was made to eliminate these through-hole related effects by plugging the hole with scattering material. This was accomplished by means of two cylindrical, 25.4 cm long pieces of reactor-grade graphite containing a 3.81 cm diameter axial hole for passage of the neutron beam and 1.27 x 1.27 cm square cable troughs on the outer diameter. A spectrographic analysis of the graphite was carried out and is reproduced in Table I. Density of this material was 1.77 g/cm^3. The effectiveness of these plugs was reflected in a 1.1% increase in tank

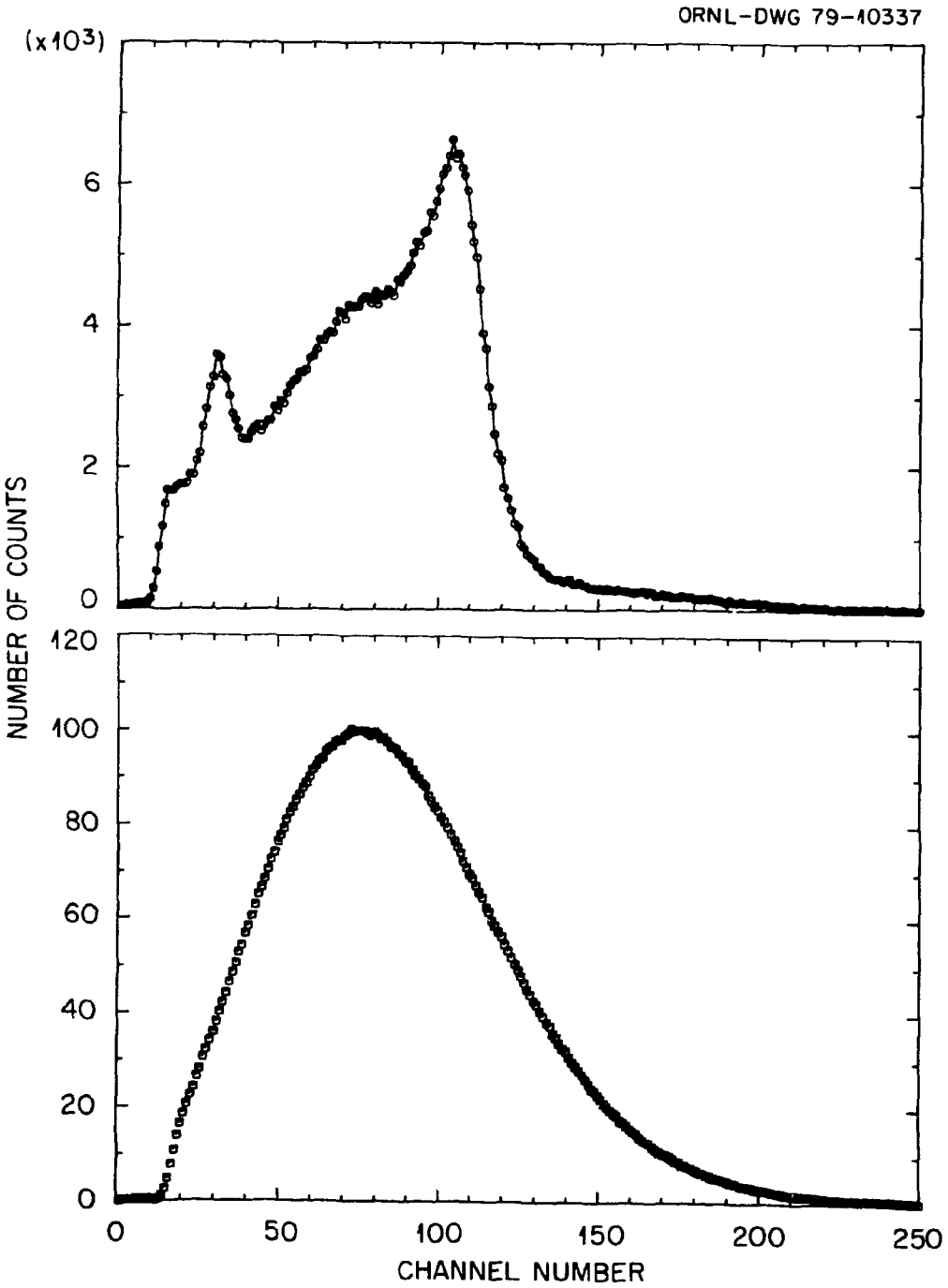

Fig. 7. Top: Pulse height spectrum of the tank due to capture of neutrons. The ADC was gated by the tank fast discriminator 4 μsec after a fission event to enhance the recording of capture γ-rays. No background has been subtracted. The line through the data points is an eye-guide only. Bottom: Pulse height spectrum of fission γ-rays in the tank. The ADC was gated with tank fast pulses occurring in coincidence with the fission chamber (no background subtraction).

TABLE I. Graphite Analysis

General Analysis (values in ppm)				Rare Earth Analysis (values in ppm)	
Ag	.05	Li	1	Y	.5
Al	10	Mg	.5	La	1
Au	< .3	Mn	.1	Ce	.5
B	.5	Mo	.2	Nd	1
Ba	10	Na	.5	Gd	.5
Be	.01	Nb	< .3	Tb	.5
Br	7	Ni	.2	Er	1
Bi	< .1	Pb	3	Yb	.2
Ca	150	Rb	< .1		
Cd	.5	Sb	< .3		
Cl	30	Sc	.5		
Co	< .1	Si	80		
Cr	2	Sn	2		
Cs	< .3	Sr	10		
Cu	.3	Ta	< .3		
Fe	10	Ti	10		
Ga	< .1	V	10		
Ge	< .1	W	< .3		
Hg	< .3	Zn	< 3		
K	1	Zr	.5		

Semiquantitative Analysis - the values reported are visual estimates taken from a standard plate and using a common graphite matrix. These values are to be interpreted as approximations only. Actual value should be within the range times 1/2 to times 2.

efficiency for ^{252}Cf neutrons (see Table II), compared to an expected direct geometrical leakage of 0.6% for the through-tube without graphite plugs.

The Proton-Recoil Detector

Calibration of the scintillator tank neutron efficiency was accomplished by scattering the ORELA produced neutron beam in a proton recoil detector. This detector consisted of a 4.45 cm diameter by 0.6 cm thick cell of NE-213 liquid scintillator mounted on a 2" RCA-8850 photomultiplier. Pulse shape discrimination was utilized with this detector to separate gamma-ray-scattered electrons from recoil proton events. The associated electronic circuit is depicted in block diagram in Fig. 8. The anode (fast) pulses from the photomultiplier were fed to an ORTEC 473A constant fraction discriminator which produced the fast logic signal used as the start to an ORTEC 467 time-to-amplitude converter (TAC). The stop input to the TAC came from a cross-over discriminator which operated on a double-differentiated linear signal. The linear signal was developed from the photomultiplier 10^{th} dynode by a TC-145 nonblocking preamplifier which fed a Canberra 1411 amplifier with 0.5 μsec delay line shaping. Figure 9 shows the linear TAC output with a ^{252}Cf source placed 1-2 cm from the NE-213 face. A window discriminator of the TAC was adjusted to cover the "neutron" peak and its output was used to tag proton recoil events for storage.

The dynode linear signal was also used for energy analysis of the proton recoil pulses. Recoil proton pulse height spectra were taken corresponding to each incident neutron time-of-flight (energy). Figures 10 and 11 show four of these spectra. The maximum proton pulse height in each spectrum (i.e. the 1/2 rise point of the spectrum high energy end) was set equal to the corresponding incident neutron energy as determined

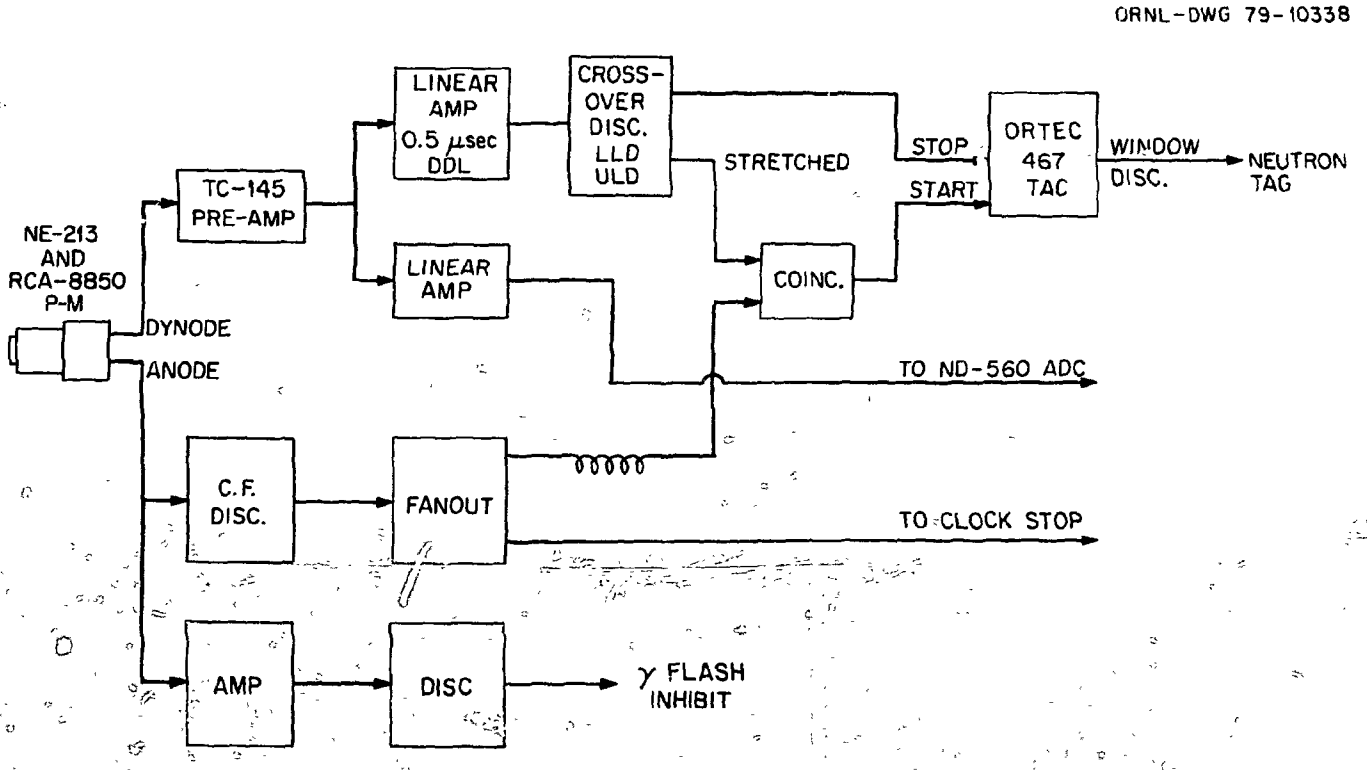

Fig. 8. Schematic diagram of the NE-213 counter pulse shape discrimination circuit.

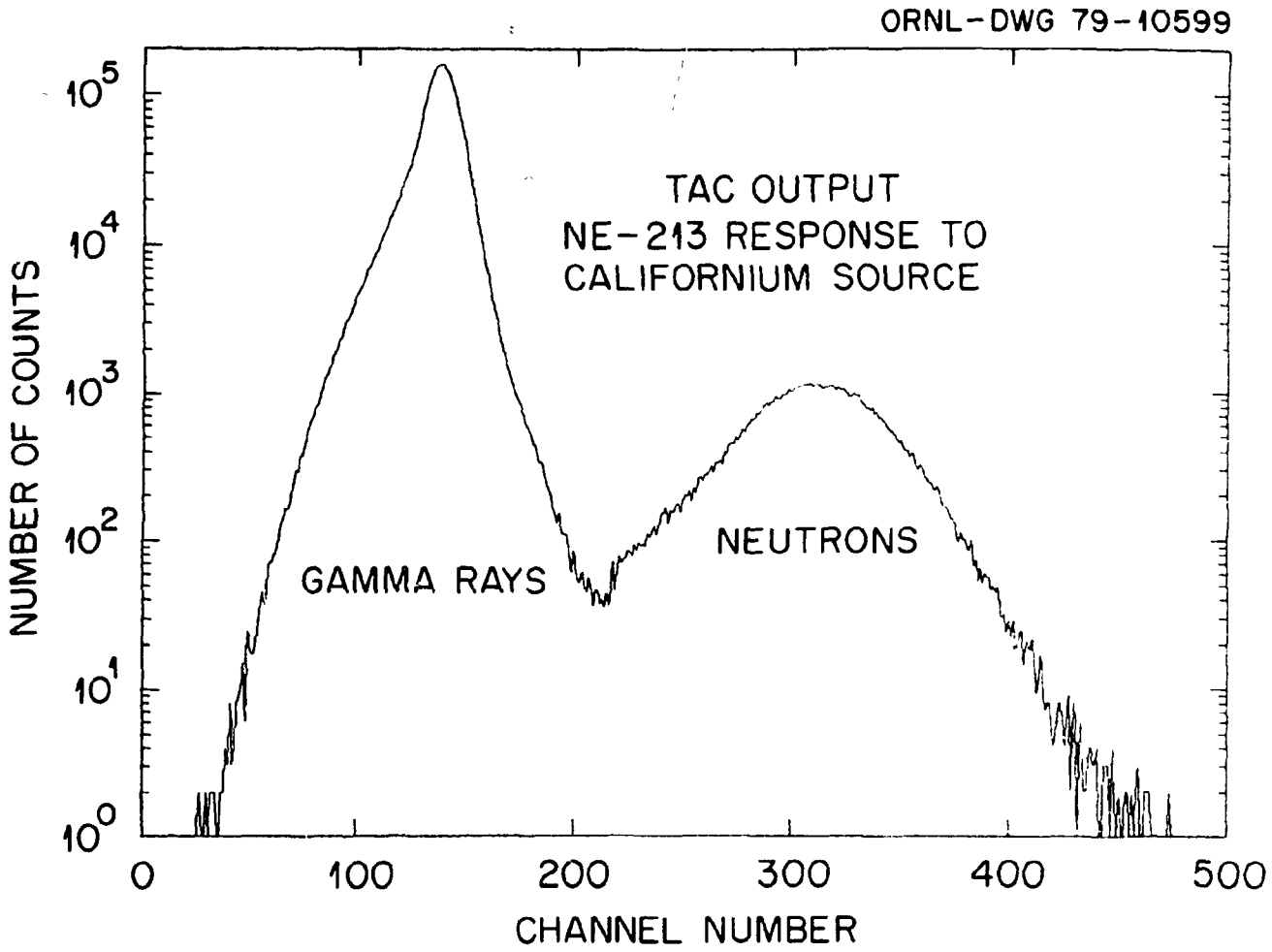

Fig. 9. Time-to-amplitude converter spectrum from the pulse shape discrimination circuit with the ^{252}Cf chamber placed near the NE-213 face. Neutron events were "tagged" by the output of a single channel window discriminator placed across the neutron peak.

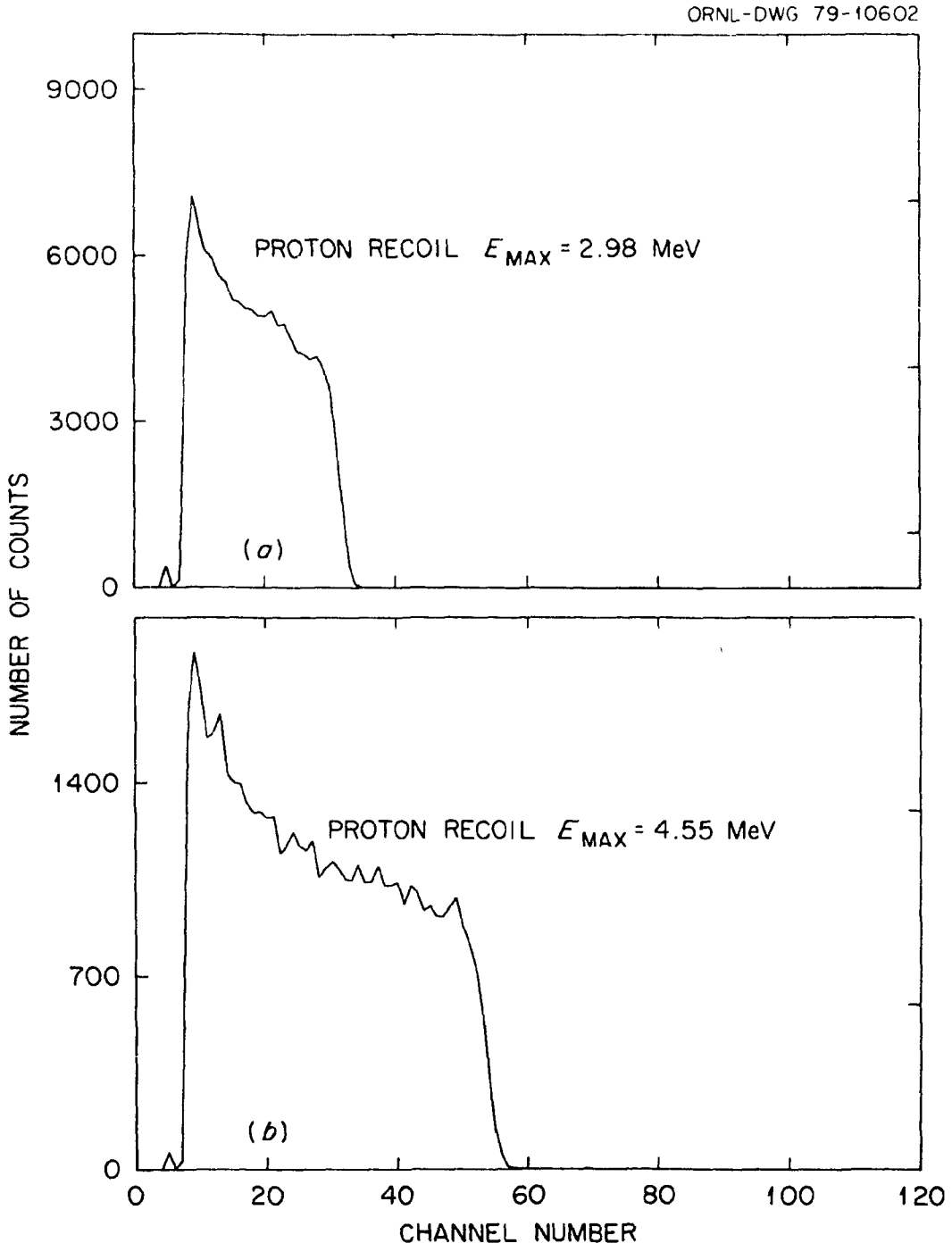

Fig. 10. Pulse height spectra of proton recoils in the NE-213 counter. Top: with 2.98 ± .10 MeV neutrons incident. Bottom: with 4.55 ± .10 MeV neutrons incident.

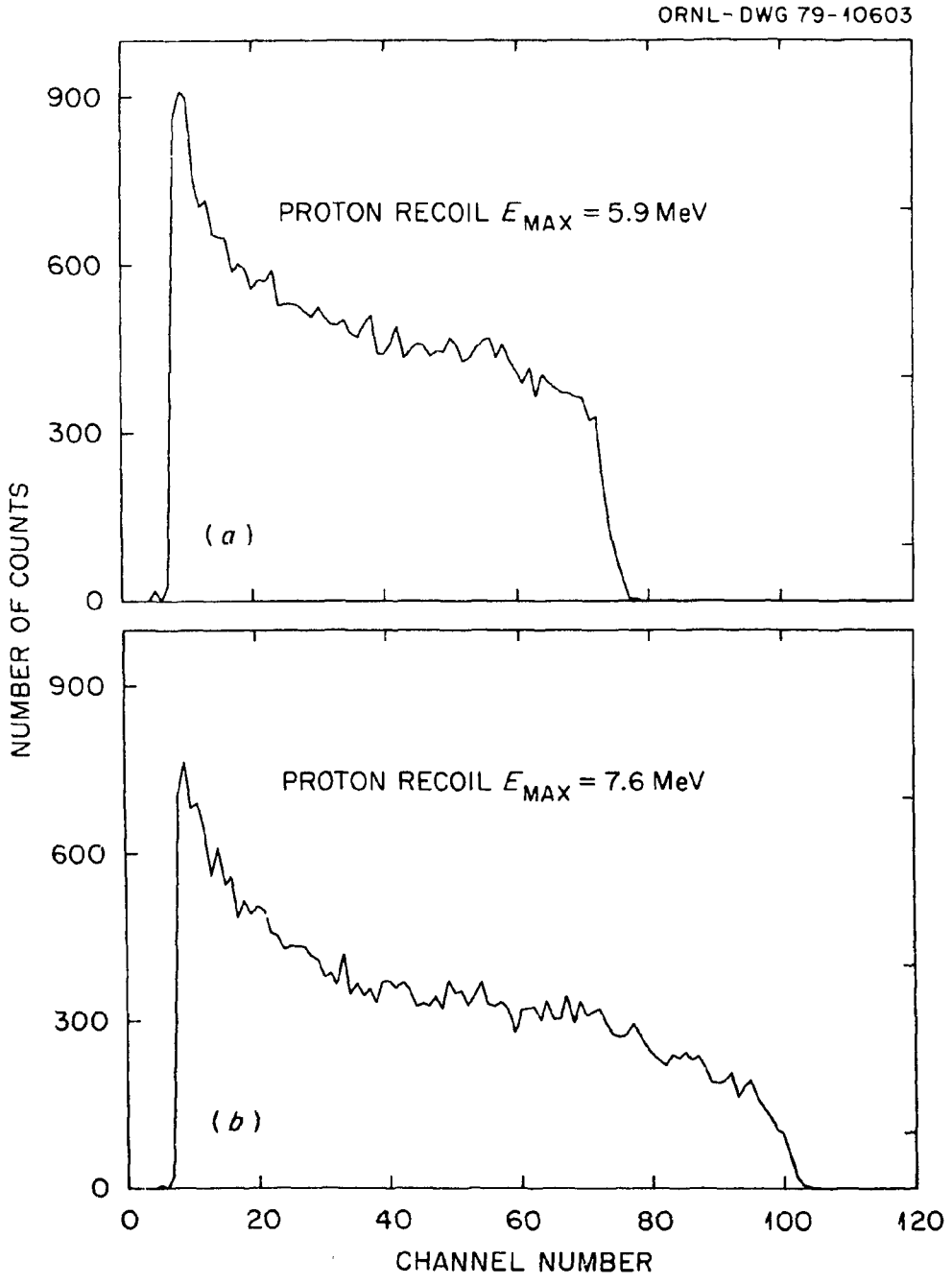

Fig. 11. Pulse height spectra of proton recoils in the NE-213 counter. Top: with 5.9 ± .08 MeV neutrons incident. Bottom: with 7.6 ± .11 MeV neutrons incident.

by time-of-flight. In this way the recoil pulse height was calibrated in 100-250 keV intervals from 1 MeV to about 8.5 MeV. Incident neutron energies were obtained from the measured flight path and the time position of the gamma flash taken with $\sim$ 0.06 nsec/meter resolution. The flight path length was checked in an auxiliary transmission measurement at this resolution by observation of the carbon 2.077 MeV resonance. Carbon resonances at 2.9, 4.3, and 6.29 MeV provided a consistency check of the neutron energy scale.

The overall effect of the pulse shape discrimination (PSD) circuit is shown in Fig. 12. In this figure the total NE-213 counts from neutrons and gamma rays is shown for all events occurring during the tank efficiency measurement up to 16 μsec after the accelerator gamma flash. Those events which had a coincident "neutron" tag from the discrimination circuit are shown as individual data points whereas the solid line represents those events which had no tag. The peak in the untagged spectrum near 3.5 μsec is due to walk in the PSD circuit and events that exceeded the upper level discriminator set at $\sim$ 8.5 MeV. The walk was adjusted so that high energy electron pulses walked away from the "neutron" window. Referring to Fig. 8, note that the constant fraction, anode pulse discriminator was set well below the crossover discriminator for proton pulses.

IV. ELECTRONICS AND DATA ROUTING

The heart of the data conversion and routing system which is shown in block diagram in Fig. 13 was an EG&G TDC-100 time digitizer with buffer memory. Events from the buffer were accumulated in approximately 280 K words of a SEL810B computer. Start pulses for the TDC-100 originated from the ORELA gamma-flash detector. The fast timing signals from each of the three detectors and the background gate generators were used to

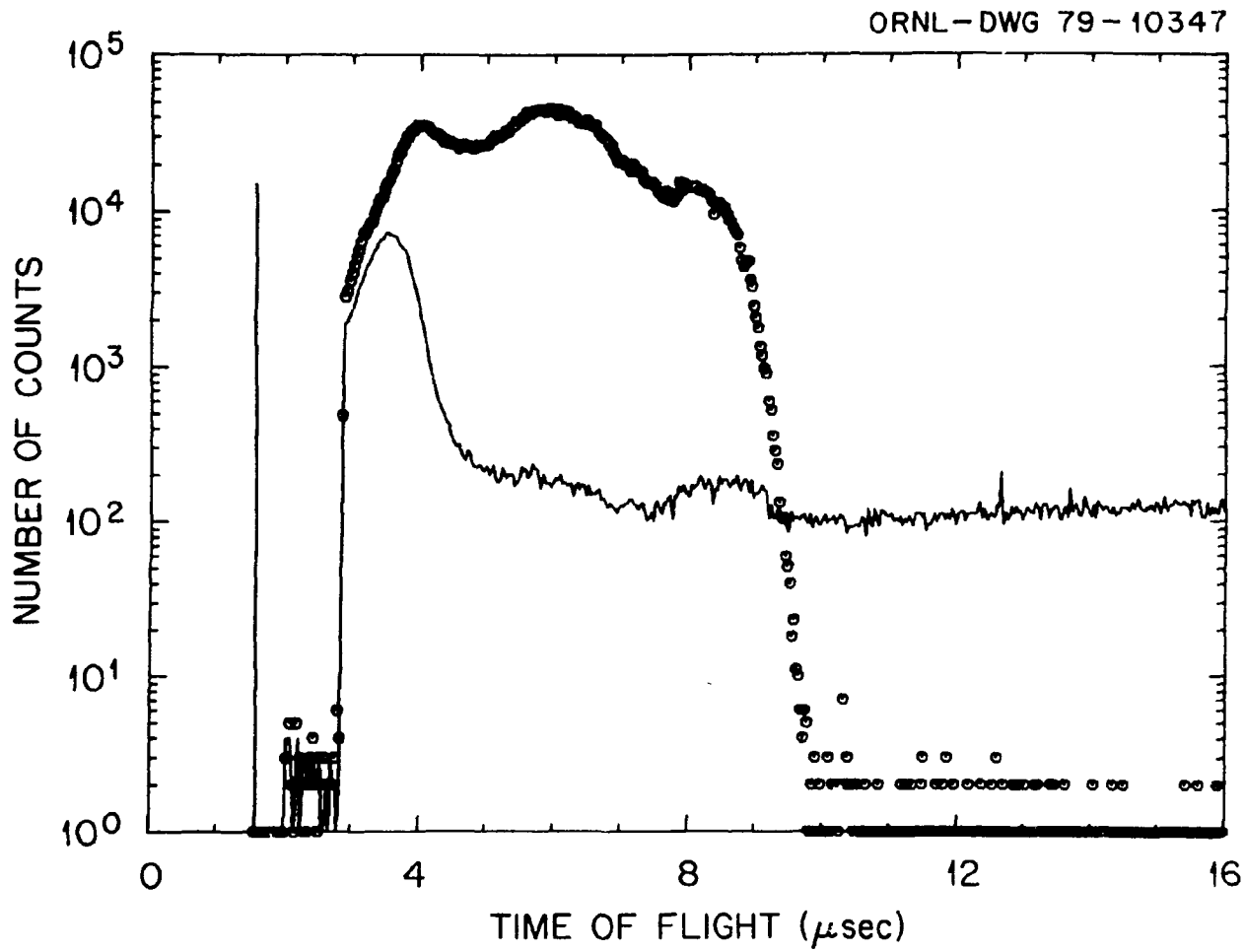

Fig. 12. Time-of-flight spectra of "tagged" neutrons (points) and discarded events (solid line) in the NE-213 detector during the efficiency measurement. One count was added to all channels of both spectra to clearly separate zero from one count on the log scale. The time-of-flight zero for neutrons in these spectra is + 1.66 μsec.

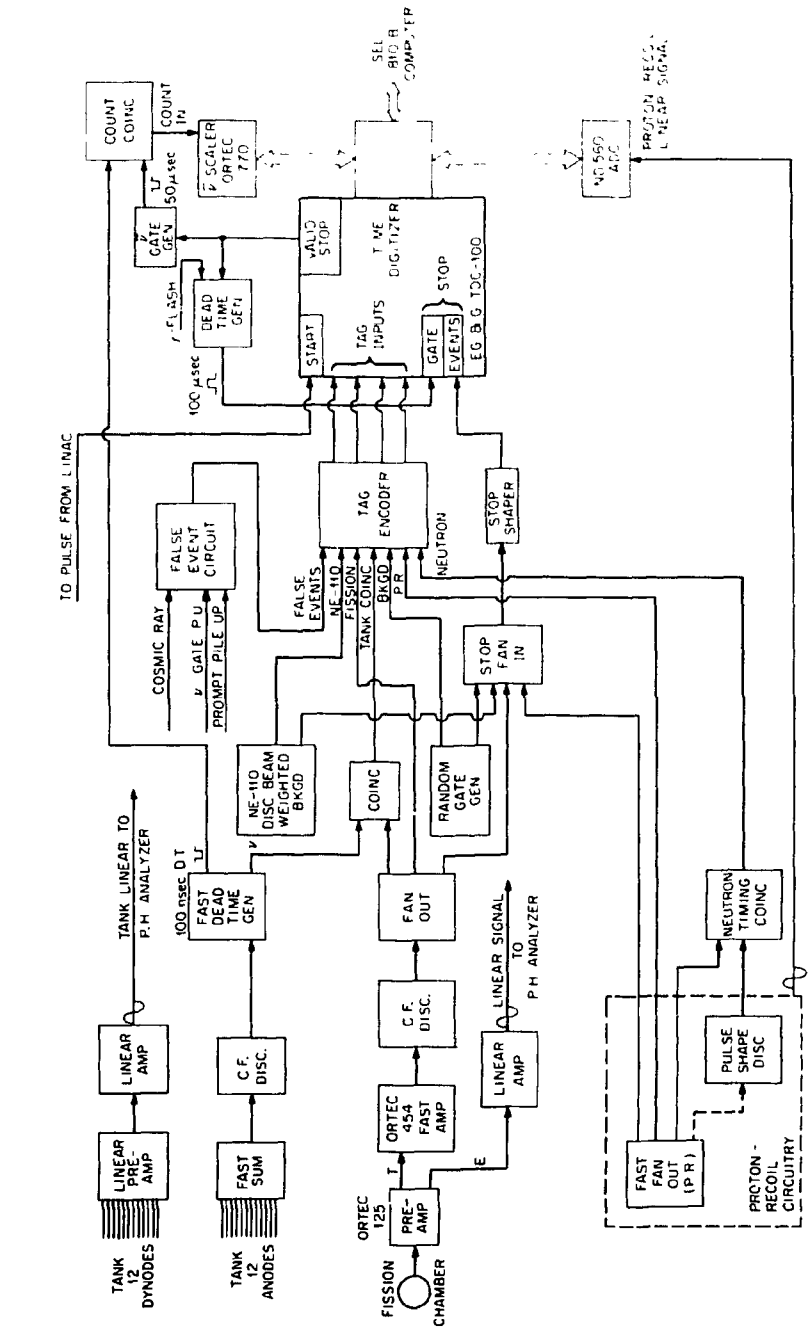

Fig. 13. Schematic circuit diagram of the measurement electronics.

stop the time digitizer. Each type of event was identified for routing to the data acquisition system by a coincident pulse which set particular "tag" bits in the TDC-100. The digitizer was operated with a 32 nsec time channel width during this experiment. In addition to event time information, the TDC-100 accepted nubar information for each event from an ORTEC 100 MHz scaler. This nubar scaler was gated to accept tank fast pulses from 0.5 to 50.5 μsec after each type of initiating event (fission, proton recoil, background). From 0 to 19 subsequent tank pulses were accepted by the TDC-100. For the proton recoil detector only, pulse height information digitized in a Nuclear Data ADC operated with 128 channel conversion gain was also fed to the TDC-100. In this way the proton recoil data were stored as a $20 \times 128 \times 64$ channel (ν vs pulse height vs time-of-flight) 3-dimensional array. Also each type of event was stored in separate 20×600 (ν vs time-of-flight) 2-dimensional arrays. One dimensional time or pulse height arrays were stored for monitoring and calibration purposes.

Part of the elaborate fast electronic system necessary for control of the experiment was devoted to the rejection of unwanted data. For example, all data were rejected for 100 μsec following cosmic ray showers in the tank (overload pulses) and for 100 μsec following detection of gamma-rays in the p-recoil counter at the time of the accelerator γ-flash. In addition, two events occurring within 100 μsec of each other were both rejected; i.e., fission events followed by a second fission or a NE-213 pulse, NE-213 events followed by a fission or another NE-213 pulse, and background gates followed by a fission or NE-213 pulse. All such events were stored in a "false events" section.

V. CALIBRATION NEUTRONS

A "white" source of neutrons used for calibration of the tank efficiency was provided by the ORELA. The electron beam was pulsed at 800/sec with a burst width of 5 ns. The average power level was 12 kW at the tantalum target. The collimation was arranged to accept a 1/2" diameter beam of neutrons coming directly from the tantalum, rather than from the surrounding water moderator, in order to enhance the flux at high energies. Filters were used to reduce the gamma-flash and to shape the neutron spectrum reaching the tank and p-recoil detector situated in the 85 M flight path bunker. The filters consisted of 0.084 atoms/barn ^{10}B, 6.8 cm ^{238}U, and 1.27 cm Pb. The drift tube from 20 meters to $\sim$ 82.5 meters was pressured to 13.8 psig with helium. The $\sim$ .3 atoms/barn of helium reduces the neutron flux in the .5 - 2 MeV energy region and results in an overall decrease in the tank background since an appreciable portion of this background comes from scattered neutrons. This system of filters limited the total count rate in the p-recoil counter to $\sim$ 75/sec of which 6/sec were neutrons, the rest primarily gamma rays from the γ-flash.

VI. BACKGROUNDS

Two types of backgrounds in the scintillator tank were determined during the measurement, random and beam-weighted backgrounds. For the random background the 50 μsec neutron counting gate was initiated by pulses from a ^{60}Co source-NaI detector system situated well away from the scintillator tank. This is the background used in the determination of neutrons from ^{252}Cf fission. In addition a background counting gate was initiated by pulses from a well-shielded neutron sensitive (NE-110)

detector situated in the neutron beam $\sim$ 5 M downstream from the tank. It is known[20] that the neutron intensity from ORELA varies from burst to burst. Thus for the p-recoil data, which depend on beam intensity, the beam-weighted background was used. This background differed by a small ($\sim$ 1.5%) but significant amount from the random background in the present experiment.

VII. DETERMINATION OF THE SCINTILLATOR TANK EFFICIENCY FOR ^{252}Cf FISSION NEUTRONS

Since n-p scattering is kinematically complete with the determination of the incident neutron energy plus the energy of one of the scattered particles, the angle of the scattered neutron with respect to its incident direction is also determined. Neglecting the n-p mass difference,

$$E_1 = E_0 COS^2\theta$$

where E_1, E_0 are scattered and incident neutron energies and θ is the laboratory angle of the scattered neutron. In the present experiment E_0 was determined by time-of-flight and E_1 is the difference between E_0 and the scattered proton energy. The scattered proton energy was determined from the recoil detector pulse height, calibrated at 64 energy values by means of the end points of the various spectra and the known incident neutron energy. Thus, the tank neutron number distributions following a proton-recoil pulse could be reduced to a distribution for a specific scattered neutron energy entering the tank at a specific angle with respect to the through-tube axis (incident beam direction). From these distributions and the background distributions for the same incident time-of-flight, the efficiency of the tank was calculated in three (not totally independent) ways for each data point. The efficiency was calculated from the foreground and background zeros, from the foreground and background one's, and for

the whole distribution ($\bar{\nu}$). The latter two required an approximate pile-up correction and were used only to check the quality of the data. From the zeros the efficiency can be written as:

$$\varepsilon(E_1,\theta) = 1 - P(o) = 1 - N(o)/B(o)$$

where ε is the efficiency and P(o), B(o), N(o) are the respective probabilities of foreground, background, and observed zeros. The efficiency results were then statistically averaged into 16 scattered-neutron energy groups and angular intervals of 5°. Due to possibility of carbon recoil effects in the NE-213 it is not practical to reach angles below about 20° and angles above about 70° could only be reached with very low energy neutrons where multiple scattering becomes large. Therefore, it was necessary to extrapolate the measured efficiencies into those regions. This was accomplished by means of Monte Carlo calculations with the code DENIS,[21] which was obtained from RSIC. The code includes both neutron and subsequent capture gamma-ray tracking. A spherical shape for the scintillator with cylindrical through-hole and scintillator volume equal to that of the actual tank were used in the calculations. Composition of the scintillator was 0.57 atomic fraction of hydrogen, 0.43 atomic fraction carbon, and 0.00008 atomic fraction gadolinium. The geometry of DENIS was revised to include the two graphite plugs in the through-hole. Neutrons were tracked until slowed to 0.1 eV at which point their energy was reset to 0.025 eV. The gadolinium capture cross section below 0.1 eV was adjusted to 36000 barns to give agreement with the exponential decay (diffusion) region of the experimental time to absorption data as shown in Fig. 14. The method of measurement of the experimental curve is explained in Section X. Scattering was assumed isotropic in

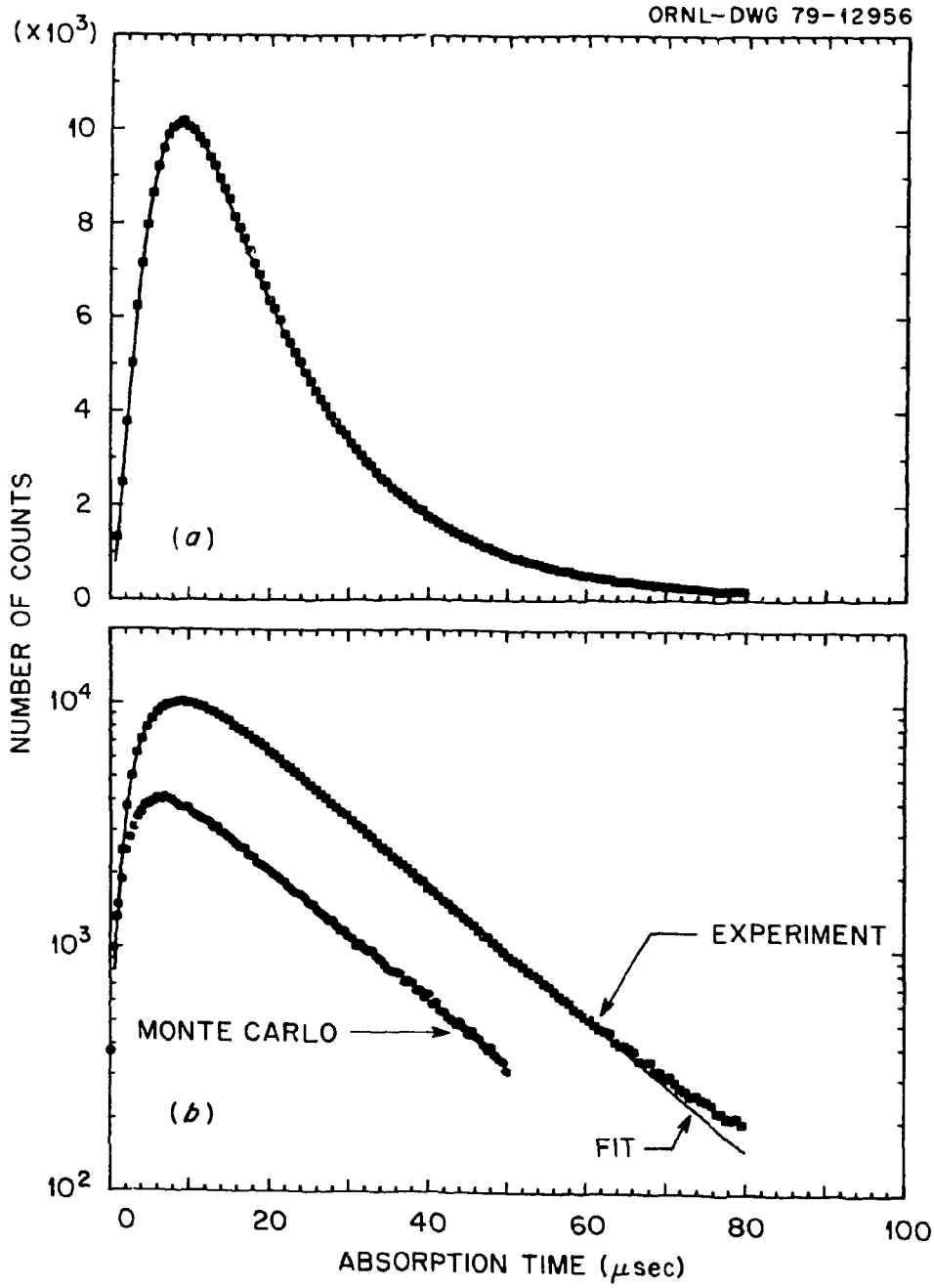

Fig. 14. Linear (a) and semilog (b) plots of the measured (square data points) fission neutron time-to-absorption distribution and a fitted function (solid line) of the form $F(t) = A(e^{-\beta t} - e^{-\lambda t}) - Bte^{-\lambda t}$ with A = 22319 ± 63, B = 6398 ± 74, β = 0.0621 ± 0.0001 and λ = 0.382 ± 0.002. The Monte Carlo predicted shape shown in the lower figure was fitted (not shown) with the same function and parameters B/A = 0.110, β = 0.0613 ± 0.0005, and λ = 0.42 ± 0.03. The units of B, λ, and β are μsec^{-1} with t in μsec.

the center of mass for all three elements in this program and the effects of the aluminum shell and photomultipliers were not taken into account. The proton recoil photomultiplier was also ignored; this required a correction which is discussed later. DENIS was then used to generate tank efficiency vs neutron energy at 5° intervals of neutron entrance angle into the tank. A least-squares fit of the calculated points to the experimental data for scattered neutrons from 1.5 to 7.1 MeV gave a normalization factor of 1.00233 ± 0.00079 to be applied to the Monte Carlo calculations. The error quoted consists of the combined counting statistics for the experimental data points and the Monte Carlo histories. Figures 15 and 16 show the normalized Monte Carlo tank efficiencies and the experimentally measured efficiencies for comparison. Of particular note in these figures is the depression of the measured efficiency below the Monte Carlo values for energy below 2.0 MeV which becomes greater for the larger scattering angles. Separate calculations of neutron absorption indicated that this effect was largely due to absorption of slow neutrons in ^{10}B present in the glass of the proton-recoil photomultiplier. Additionally, it was found that removal of the proton-recoil detector resulted in an increase in the observed ^{252}Cf $\bar{\nu}$ of 0.35%. With a .030" thick cadmium liner in the through-tube, removal of the recoil detector resulted in only a 0.09% increase in observed $\bar{\nu}$. This is further evidence that the effect is one of slow neutron absorption and not due to disturbance of the tank capture gamma rays by the recoil detector. Since the code DENIS did not contain the recoil detector the following, not totally satisfying, procedure was used to eliminate the ^{10}B effect from the calibration. All efficiency data for scattered neutron energies of 0.5 and 1.0 MeV in addition to the three highest scattering angle data points at 1.5 MeV were

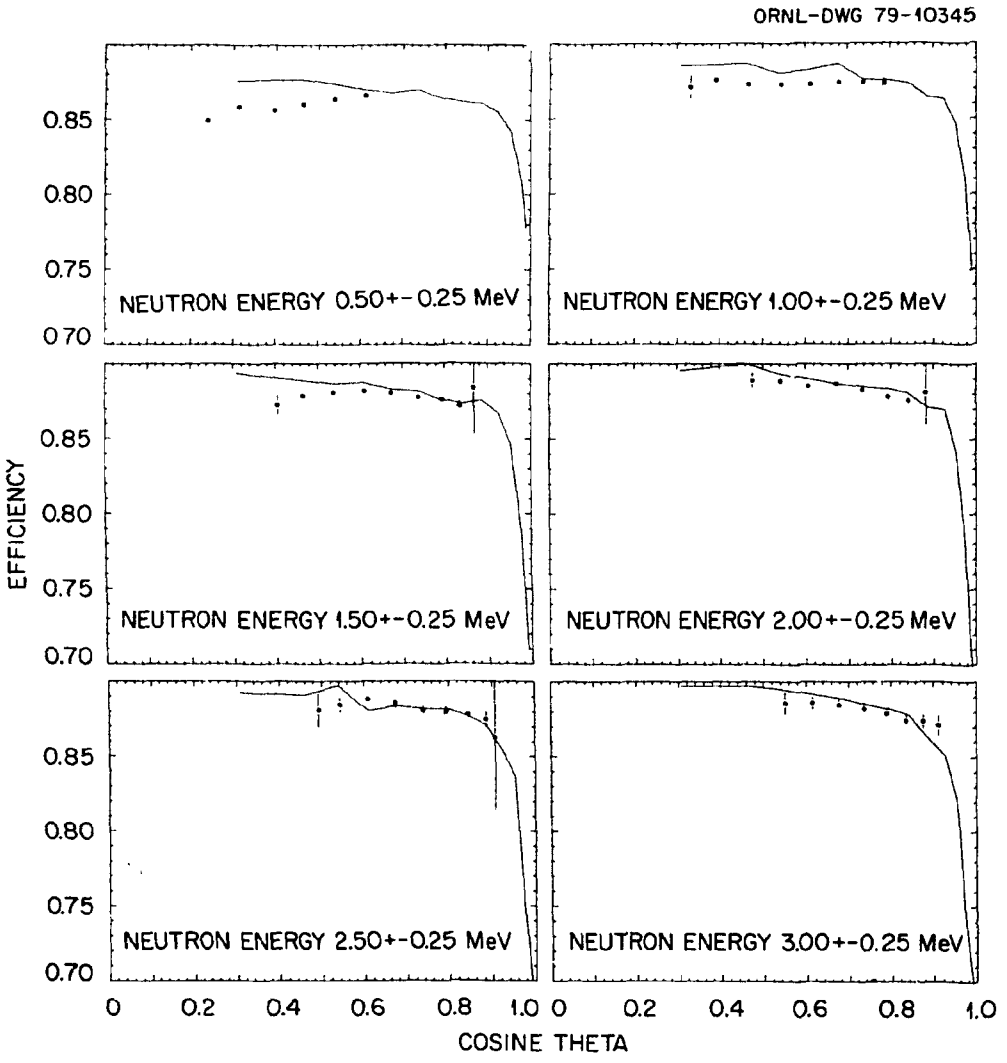

Fig. 15. Experimental (points) and Monte Carlo calculated (lines) tank efficiencies for neutrons from 0.5 to 3.0 MeV energy vs cosine of the neutron scattering angle. The Monte Carlo calculations were carried out for 5° intervals in scattering angle with 10,000 histories at each angle. Straight lines are used as eye guides between the calculated data. Where error bars are not visible in the experimental data, they are of the size of the data points.

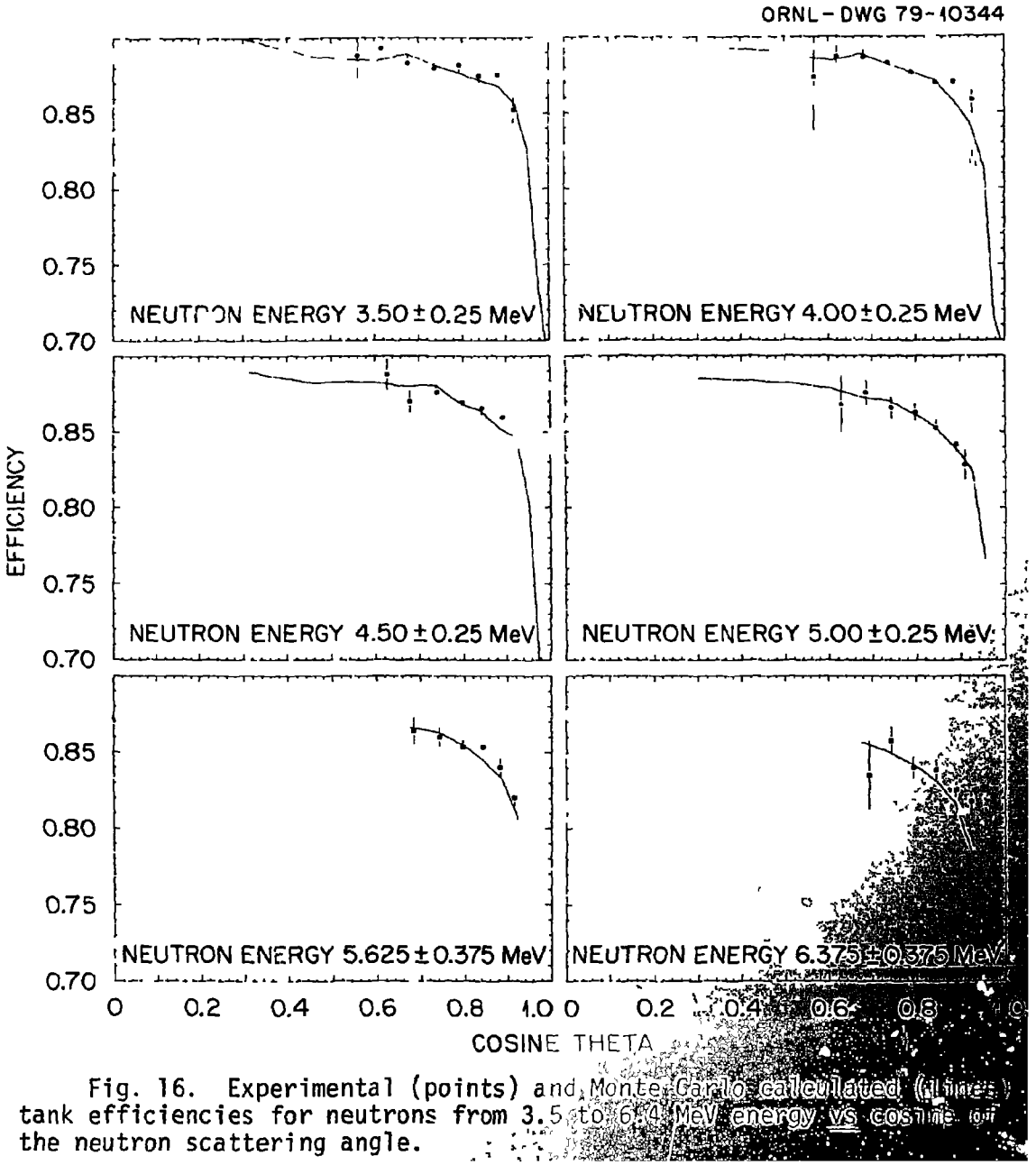

Fig. 16. Experimental (points) and Monte Carlo calculated (lines) tank efficiencies for neutrons from 3.5 to 6.4 MeV energy vs cosine of the neutron scattering angle.

discarded in obtaining the normalization factor given above. DENIS was then used to calculate the total tank neutron efficiency for an isotropic Maxwellian distribution ($\bar{E}$ = 2.09 MeV) in a 17 energy group structure. The total tank efficiency obtained for ^{252}Cf neutrons after multiplication by the normalization constant was 0.8713 ± 0.0013. Here the error consists of the combined errors in the normalization constant and the counting statistics for the Monte Carlo calculation for the isotropic, Maxwellian source. A Monte Carlo calculation of tank efficiency vs neutron energy using the correct conical shape of the outside shell is shown in Fig. 17. A decrease in efficiency at low neutron energies is predicted which, according to DENIS, is due to a higher fraction of neutrons with low initial energies being captured at times longer than the 50 μsec counting interval. This effect would seem to be a result of the traversal time of thermal neutrons in the through-tube and the shorter thermalization mean-free path of neutrons with lower initial energies. Further evidence was obtained in measurements of time-to-absorption taken with a cadmium through-tube liner. A significantly shorter thermal diffusion time constant was observed with cadmium than shown in Fig. 14 for the bare through-tube. Both this effect and the ^{10}B absorption in the recoil detector can be alleviated to a high degree by using a cadmium liner in the through-tube (or a much higher gadolinium concentration), and a smaller through-tube. These changes are planned for a future measurement.

The effect of the graphite plugs was investigated both experimentally and by calculation with DENIS. Observed $\bar{\nu}$'s for the ^{252}Cf chamber were recorded with and without the plugs. The ratio of these two $\bar{\nu}$ values is compared in Table II with that calculated for the ^{252}Cf source by DENIS. The agreement is seen to be very good.

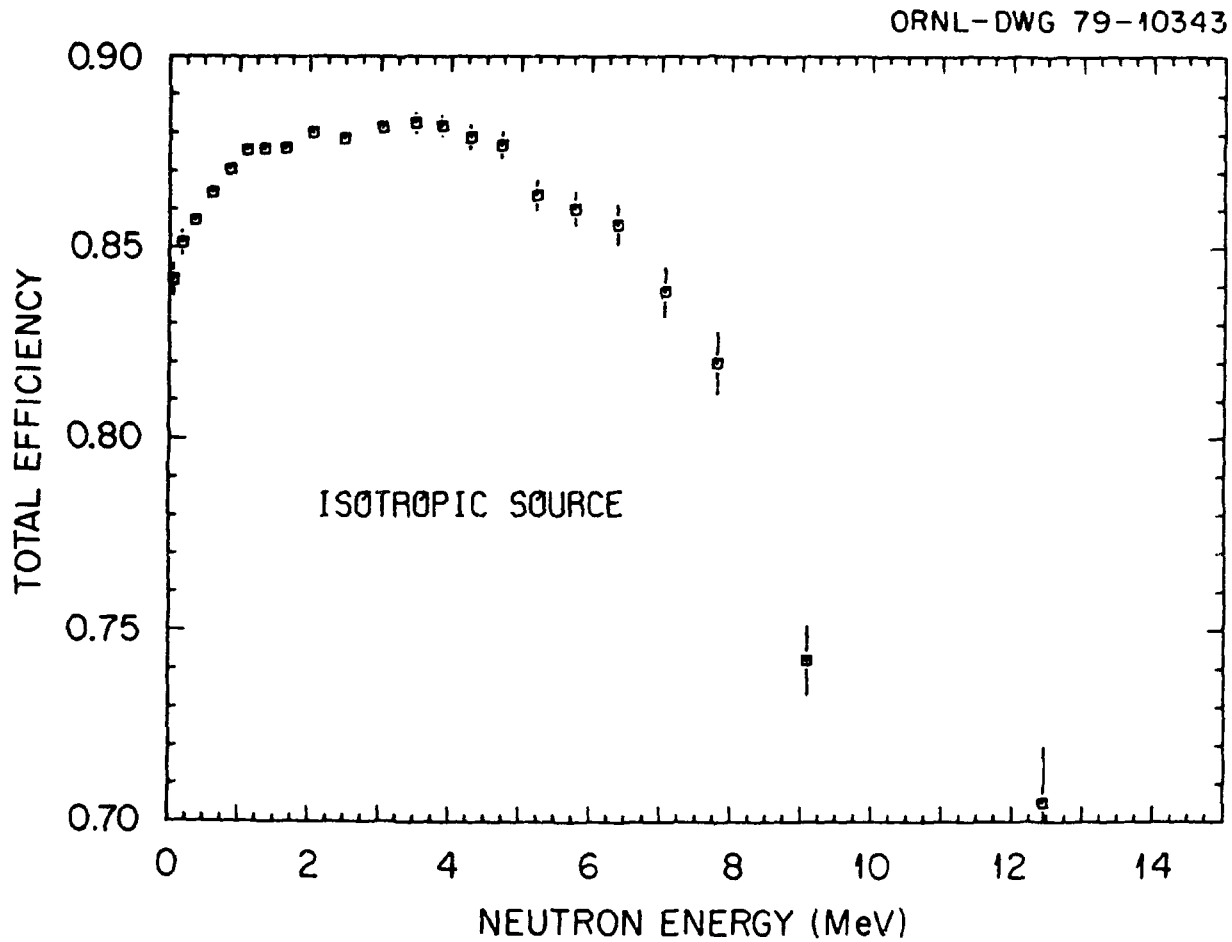

Fig. 17. Monte Carlo calculated total efficiency of the scintillator tank for isotropic neutrons vs neutron energy. The calculation was for 400,000 total histories, weighted by a Maxwellian with average energy of 2.09 MeV.

The proton-recoil data were also checked for evidence of multiple pulsing of the discriminator and afterpulsing of the nubar tank photomultipliers both of which would lead to an excess of twos in the scattered neutron data. The proton recoil data for all energies and angles were added and the resulting neutron distribution corrected for pile-up and stripped of background (beam-weighted). The results, shown in column three of Table III, are clearly indicative that no multiple or afterpulsing exists, at least following neutron capture in the tank. These results do not rule out an effect in the californium data following the tank prompt fission gamma-ray response. However, no evidence was observed of any time correlated peak in the tank response following prompt fission gamma rays. Table III also shows the effect of using the random background in correction of the proton-recoil data in column two. This distribution contains an excess of twos but interestingly enough, very little effect on the zeros. Since only the zero's probabilities were used to obtain the tank efficiency, it is likely that little error would have resulted in the present experiment had the random background been used exclusively. For higher backgrounds the error increases, however.

VIII. REDUCTION OF THE ^{252}Cf NEUTRON DATA

The value of nubar determined in this type of measurement is given simply by

$$\bar{\nu} = \frac{\bar{n} - \bar{n}_{BKGD}}{\varepsilon} , \qquad (1)$$

where

$$\bar{n} = \sum_{n=1}^{\infty} n\, N'(n) \ , \ \bar{n}_{BKGD} = \sum_{n=1}^{\infty} n\, B'(n)$$

TABLE II

	with Graphite/without
Monte Carlo	1.0113 ± 0.0009
Experiment	1.0114 ± 0.0005

TABLE III. Calibration-Neutron Number Distributions

n	Q(n) (Random Bkgd.)	Q(n) (Beam Wt'd. Bkdg.)
0	0.147609	0.147918
1	0.850678	0.852166
2	0.001712	0.000001
3	0.000007	-0.000097
4	-0.000000	0.000009
5	-0.000003	0.000011
6	0.000004	-0.000004
7	-0.000011	-0.000005
8	0.000006	0.000000
9	0.000000	0.000000
$\bar{n}$	0.854101	0.851913
Statistical Error	±0.00026	±0.00026

are the observed average number of events per fission-triggered gate and per background gate, respectively, corrected for system deadtime and ϵ is the average tank efficiency for detection of ^{252}Cf neutrons. For Poisson statistics the pile-up correction requires only the average rates and the system deadtime per pulse. However, the absorption of more than one neutron per gate introduces correlations, is therefore non-Poisson, and the pulse pile-up correction requires, in addition, the neutron number probability distribution and a measurement of the time distribution of neutron absorption within the gate. Correction of the fission data for a single pulse overlap per gate has been discussed by Diven et al.[22] The prescription given in ref. 22 was followed with modification for two pulse overlaps per gate given by Frehaut[23] plus an approximate expression for triple pile-up events. These latter two corrections had a negligible effect. Thus, for the case of a single overlap of two neutrons the observed neutron number probabilities are given by:

$$N(n) = N'(n)\{1 - C_n^2 k_2\} + N'(n+1)C_{n+1}^2 k_2 \qquad (2)$$

and for the background probabilities

$$B(n) = B'(n)\{1 - C_n^2 k_{2B}\} + B'(n+1)C_{n+1}^2 k_{2B} \qquad (3)$$

where the primed quantities refer to the corrected distributions and k_2 or k_{2B} are the probabilities that two neutron or two background pulses, respectively, are coincident within the system deadtime. C_n^2 and C_{n+1}^2 in Eqs. (2) and (3) are binomial coefficients. Nubar can then be obtained from Eq. (1). The background stripping and derivation of the neutron number distribution corrected for efficiency can be carried out again following ref. 22:

$$N'(n) = \sum_{i=0}^{n} Q(n - i)B'(i) \tag{4}$$

and

$$P(\nu) = \sum_{n=\nu}^{\infty} C_n^{n-\nu}(1 - \frac{1}{\varepsilon})^{n-\nu}(\frac{1}{\varepsilon})^{\nu} Q(n) \tag{5}$$

where the $C_n^{n-\nu}$ are again binomial coefficients and ε is the average detector efficiency for ^{252}Cf neutrons. If the value of ε varied with neutron numbers (for example if the neutron energy were correlated with neutron number) equation (5) could yield an erroneous number distribution but the value of nubar derived is still given by:

$$\bar{\nu} = \frac{1}{\varepsilon} \sum_{n=0}^{\infty} nQ(n) \tag{6}$$

where ε is the average efficiency for fission neutrons. The similarity of derived neutron number distributions given here and by other investigators using detectors of different size is evidence against any strong correlation of this type.

In the present experiment ^{252}Cf neutron multiplicity distributions were derived corresponding to two time-of-flight regions of neutrons incident on the p-recoil detector. These are shown in Table IV. The lower background data (A) correspond to the time-of-flight region from 12.8 to 218 μsec after the linac gamma-flash whereas the higher background data (B) were taken from 1.2 to 12.8 μsec after the flash (the time region of p-recoil events). Agreement in the $\bar{\nu}$ values obtained as above and with $\bar{\nu}$ observed during shutdown of the linac indicate negligible short or long term effects on the tank or its electronics attributable to linac-induced noise or irradiation.

TABLE IV. ^{252}Cf Neutron Number Distributions

	n	N(n)	B(n)	Q(n)
			Low Background	
	0	0.007753	0.942704	0.008224
	1	0.062226	0.054929	0.064428
	2	0.195498	0.002200	0.199538
	3	0.302628	0.000124	0.305531
	4	0.256140	0.000025	0.254832
	5	0.127136	0.000010	0.123200
	6	0.039434	0.000004	0.036533
	7	0.007985	0.000002	0.006852
	8	0.001077	0.000001	0.000795
	9	0.000110	-	0.000064
	10	0.000010	-	0.000002
Gates		26,009,680	14,574,573	
$\bar{n}$		3.32359	0.059900	†3.28954 ± 0.00029
$\sigma^2(n)$				1.6556
R				-0.15100 ± 0.00011
			High Background	
	0	0.006962	0.852322	0.008168
	1	0.056981	0.135274	0.064419
	2	0.182757	0.011378	0.199712
	3	0.292298	0.000826	0.305961
	4	0.259563	0.000130	0.254134
	5	0.139470	0.000046	0.123275
	6	0.048251	0.000020	0.036471
	7	0.011530	0.000003	0.007064
	8	0.001873	0.000003	0.000699
	9	0.000281	-	0.000110
	10	0.000030	-	-0.000011
Gates		1,368,603	767,906	
$\bar{n}$		3.42307	0.161412	†3.2893 ± 0.0011
$\sigma^2(n)$				1.6579
R				-0.15081 ± 0.00049

†The original pile-up factor (k_2 = 0.005378) obtained from the time of absorption curve was used here. Note the correction to this mentioned later.

IX. STATISTICS

Mather[24] has given for the variance of the average value corresponding to an observed distribution:

$$\sigma_{\bar{n}}^2 = \left[\sum_{n=0}^{\infty} n^2 g_n - \left(\sum_{n=0}^{\infty} n g_n\right)^2 \Big/ \sum_{n=0}^{\infty} g_n\right] \Big/ \left(\sum_{n=0}^{\infty} g_n\right)^2 \qquad (9)$$

where g_n is the number of gates in which n counts are observed. This equation reduces to:

$$\sigma_{\bar{n}}^2 = [\langle n^2 \rangle_{avg} - \langle n \rangle_{avg}^2]/\text{Total Gates} \qquad (10)$$

and can be used to compute the counting statistical error in both the average counts per fission gate or background gate. The variance in the background-subtracted observed nubar value is then just the sum of the variances for the fission gated and background gated average counts. It was assumed that the estimated error in the pile-up correction can be independently accounted for.

Another form of variance derivation is of interest. Given the real nubar distribution with natural width σ_ν, the variance of the observed distribution using a detector with average efficiency ε is

$$\sigma_n^2 = \varepsilon^2 \sigma_\nu^2 + \varepsilon\bar{\nu}(1 - \varepsilon) \qquad (11)$$

Dividing both sides by $\bar{n}^2$ and recalling that $\bar{n} = \varepsilon\bar{\nu}$, equation (11) becomes with some re-arrangement:

$$\frac{\sigma_n^2}{\bar{n}^2} - \frac{1}{\bar{n}} = \frac{\sigma_\nu^2}{\bar{\nu}^2} - \frac{1}{\bar{\nu}} = R \qquad (12)$$

where R is an invariant of the system with respect to changes in neutron detection efficiency. This feature of R is a valuable monitor of the

detector performance.[22,25] The variance of the observed nubar may also be written using Eq. (11) for the case of no background:

$$\sigma_{\bar{n}}^2 = \frac{1}{G_F} [\varepsilon^2 \sigma_\nu^2 + \bar{n}(1 - \varepsilon)] \tag{13}$$

where G_F is the total number of fission gates. Thus, a reasonable knowledge of σ_ν^2 permits an estimate of the variance of the observed nubar for given values of detector efficiency. This form with inclusion of background terms and $\sigma_\nu^2 \sim 1.6$ was found to give good agreement with the similar statistic obtained from Eq. (10).

For counting of proton recoil neutrons binomial statistics apply and the variance in the measured neutron efficiency is given as:

$$\sigma_\varepsilon^2 = \frac{1}{G_p} [\varepsilon(1 - \varepsilon)] \tag{14}$$

where ε is the observed efficiency when G_p total neutrons enter the detector and background effects have been neglected. This is equivalent to Eq. (10) for the case of n = 0 or 1 only.

X. CORRECTIONS TO THE ^{252}Cf DATA

In addition to the major correction of the data for the detector neutron efficiency, a number of secondary corrections have been recognized that are indigenous to the scintillator tank technique (e.g. see Refs. 3 and 24). These corrections, along with two others that arose in the present experiment, and their contribution to the uncertainty in the final result are discussed below in the order in which they were applied. Several of the effects required separate measurements, which in general were made following the efficiency determination.

Pile-up Correction

The pulse overlap probabilities used in the pile-up correction of the californium and random background nubar data were derived from the following equations:

$$k_2 = 2\tau \int_{T_o}^{T_o+T} f^2(t)dt, \text{ two neutron overlap} \tag{15}$$

$$k_3 = 3\tau^2 \int_{T_o}^{T_o+T} f^3(t)dt, \text{ three neutron overlap} \tag{16}$$

$$k_{2B} = 2\tau/T, \text{ two background pulse overlap} \tag{17}$$

$$k_{3B} = 3\tau^2/T^2, \text{ three background pulse overlap} \tag{18}$$

where τ is the system deadtime (nonextending), T_o is the time after fission that the neutron counting begins, T is the length of the counting interval, and f(t) is the normalized time-of-absorption distribution. The overlap probability of a neutron with a background pulse is the same as for two background pulses.

The counting interval gate length was observed on a calibrated oscilloscope to be T = 50.0 ± 0.5 μsec. The counting interval began 500 ± 20 nsec after a fission or background gate. These uncertainties lead to $\leq$ 0.5% and 1.0% uncertainties in k_2 and k_{2B}, respectively. Since the same counting interval gate was initiated by either fission events or the background generator, no systematic error arising from mismatch of counting interval lengths exists.

The time distribution of neutron absorption was measured in a separate experiment using the californium chamber as a source of neutrons and the EG&G TDC-100 digital clock coupled with the SEL computer to process and store events. The time data were stored according to the number of events registered in the nubar scaler for a time period of 80 μsec after a fission (determined by a coincidence between the tank and the fission ion chamber). The clock deadtime for multiple "neutron" events occurring in the counting interval was 1 μsec. Figure 14 shows the time-of-absorption data observed (squares) when only one event was registered in the nubar scaler. The clock time resolution was 64 nsec per channel and the average background was $\sim$ 9.5 counts per channel. The integrals of Eqs. (15) and (16) were evaluated from this data between 0.5 and 50.5 μsec after fission. The counting statistical errors in evaluation of the integrals were negligible.

The natural deadtime of the liquid scintillator tank was $\sim$ 60 nsec. This is determined primarily by the width of the summed fast pulses and to some degree by the properties of the constant fraction trigger on the output of the sum device (see Fig. 13). This natural deadtime is exemplified in the top spectrum of Fig. 18, which shows the pulse height

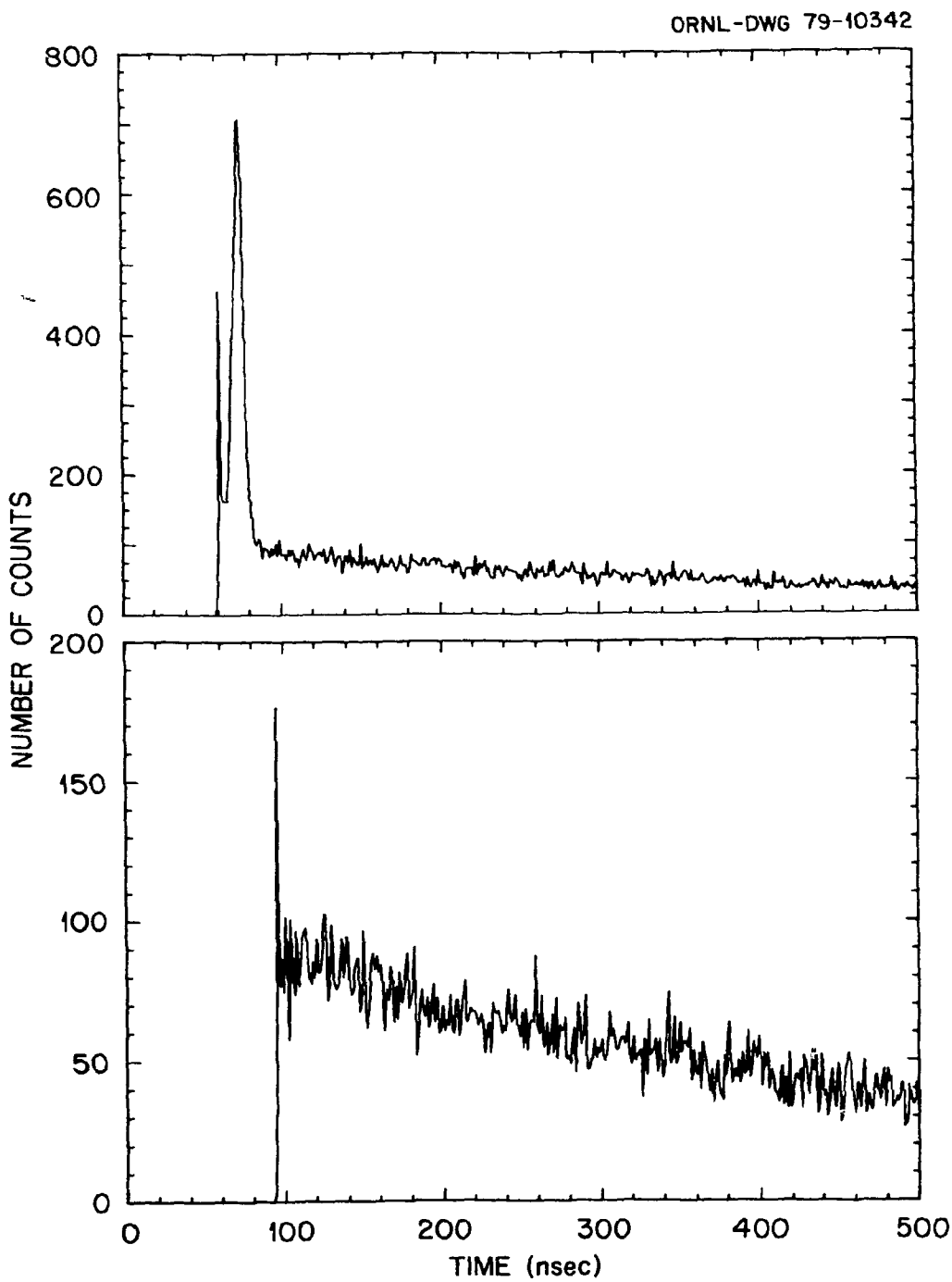

Fig. 18. Time spectra of events following a background event in the tank, i.e. interval distributions. Top: with minimum deadtime ($\sim$ 5 ns) in the T-105 tank fast discriminator to show the natural deadtime of the tank constant fraction discriminator system. Bottom: with a 95 ns imposed deadtime in the tank fast discriminator as was used in the experiment to eliminate multiple pulsing.

output of a time-to-amplitude convertor (TAC) operating on tank fast pulses under ambient background ($\sim$ 800/sec) conditions. The TAC was started with any tank fast pulse and was stopped by the next subsequent tank fast pulse. Sensitivity was 1.18 nsec per pulse height channel as calibrated with a precision pulser. Enhancement of the first "live" channel is due to pulse rise time effects. The large peak occurring at $\sim$ 75 nsec is caused by retriggering of the constant fraction device on noise, etc., plus the tail of the initializing pulse which has not yet reached baseline (i.e. the tank fast pulse widths at the constant fraction triggering level of $\sim$ 80 MV are greater than 60 nsec but much less than 100 nsec for all pulses below saturation). In order to prevent any retriggering capability, an EG&G T-105 trigger with a $\sim$ 100 nsec shaping cable was introduced at the output of the constant fraction device. The lower spectrum of Fig. 18 shows the effect of the T-105 deadtime trigger. A system deadtime $\tau = 95.3 \pm 1.2$ nsec for use in the pile-up correction was determined from this latter data. The overlap probabilities were then calculated to be:

$$k_2 = 0.005378, \quad k_{2B} = 0.003812,$$

$$k_3 = 0.000025, \quad k_{3B} = 0.000011.$$

The indication of longer term structure in the time interval distributions of Fig. 18 led to a number of studies to include intervals as long as $\sim$ 1000 μsec. For these studies the TDC-100 was used as a time digitizer with 4 nsec per channel resolution and in the multiple-stop per start mode with 1 μsec deadtime (this led to negligible counting losses at the rates encountered). The time interval distribution under

ambient background conditions is shown in Fig. 19. Two types of structure appear. at early times a component with $T_{1/2} \sim 350$ nsec and at longer time intervals, a few tens of microseconds component. The former may be due to radiative μ^- capture in $Z \sim 20$ nuclei[26,27] and the latter to neutrons from cosmic ray interactions near or in the tank. That these structures are correlated events rather than some manifestation of the fast electronics can be seen in Fig. 20. This time interval distribution was taken by starting the TDC-100 at the time of firing of a red light-emitting-diode (LED) mounted in the tank. Stops again were subsequent tank pulses. The LED was operated at a 1000 Hz rate and resulted in a pulse height in the tank equivalent to 1.5 to 2 MeV energy. Similar flat time interval distributions were observed for LED pulse heights of greater than 10 MeV and for a ^{60}Co source ($\sim$ 7000 disintegrations/sec) in the tank but no LED. On the other hand the time interval distribution taken with a ^{22}Na source (β^+ emitter) adding 700 counts/sec to the tank ambient rate, Fig. 21, showed an early structure with $T_{1/2} \sim 140$ nsec. This half-life is characteristic of free decay of the triplet state of positronium. The 350 nsec component was not affected by elimination of all pulses above 12 MeV, so it is not certain if it is correlated with cosmic showers. In summary, although the structures remain only tentatively identified, there is no indication that they would not be properly taken into account in either the background determination for nubar or in the tank neutron efficiency measurements. The evidence is strongly against afterpulsing, multiple pulsing, or a long decay light component in the tank scintillator.

As a final test of the pile-up correction technique nubar data were taken for the californium source as a function of system deadtime.

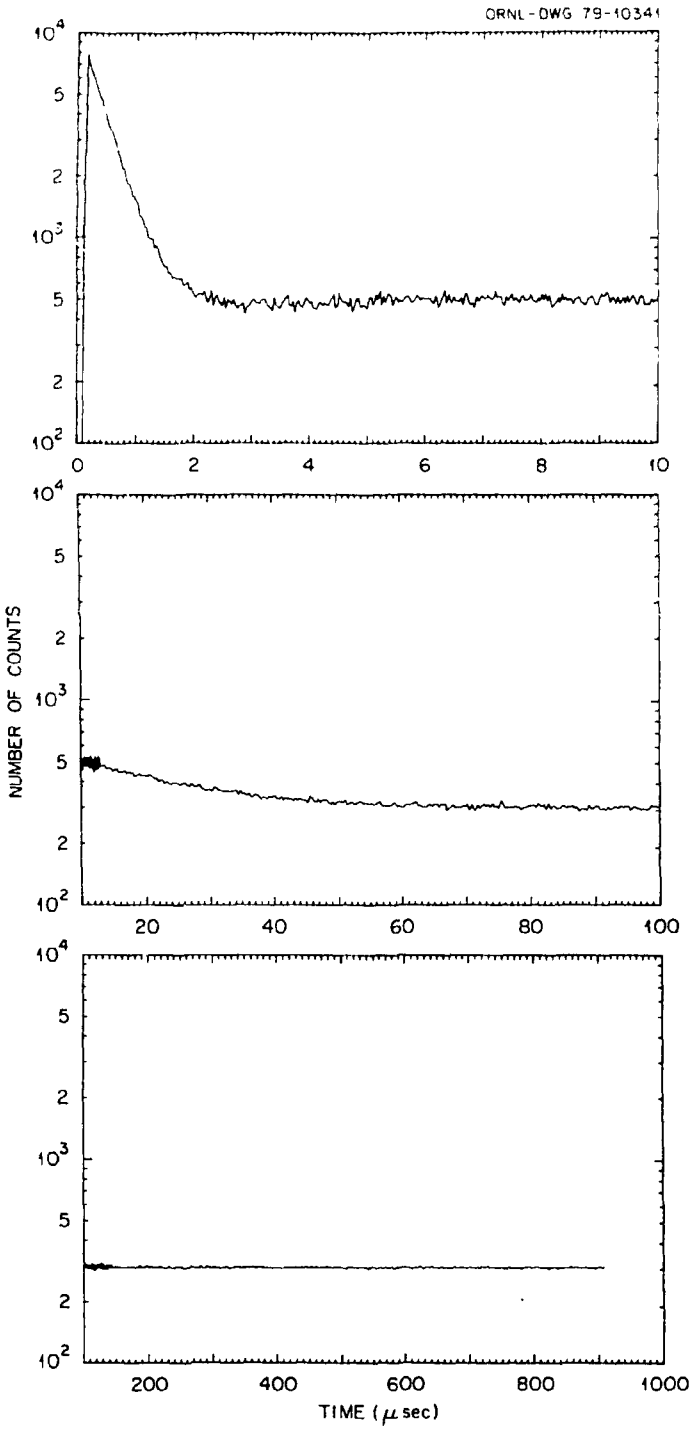

Fig. 19. Time distribution of tank events triggered by a background pulse showing correlated event structures at early times (∿ 340 nsec decay) and out to a few 10's of μsec due probably to neutrons from cosmic ray interactions in or near the tank. At long times the distribution is flat at a level characteristic of the random rate. Discriminator deadtime was 95 nsec.

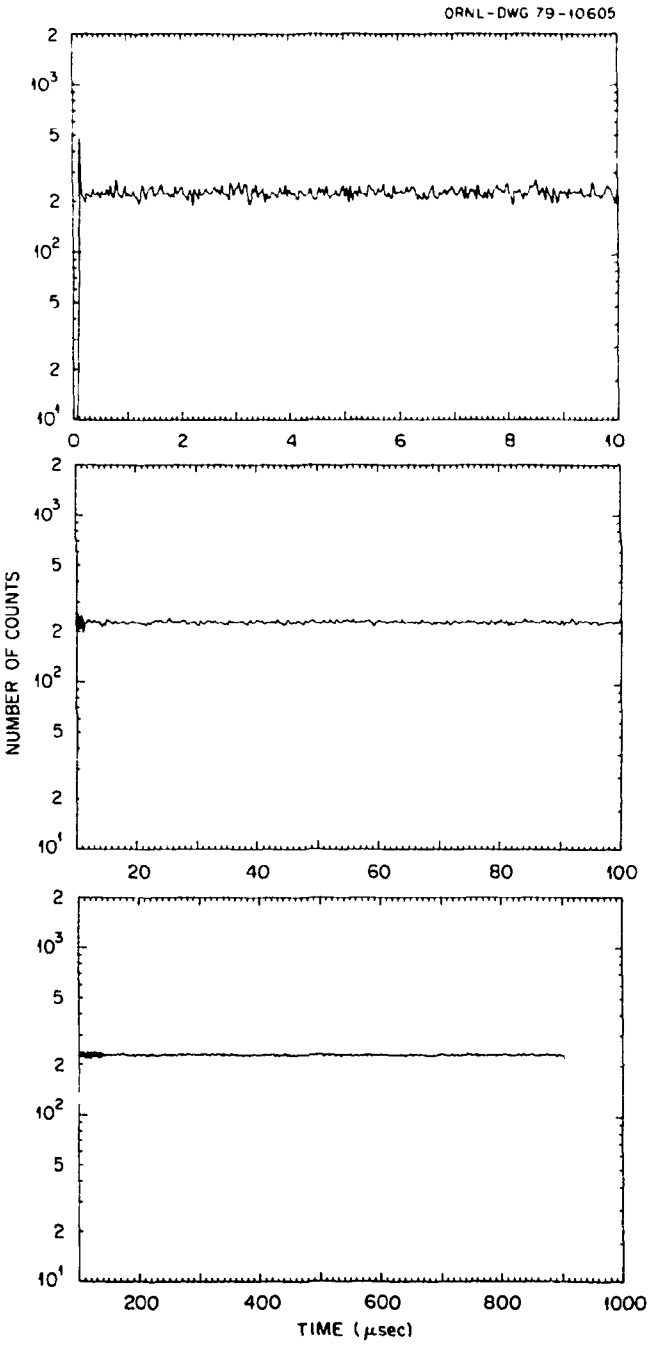

Fig. 20. Time distribution of tank events following a tank LED excited scintillator emission. The distribution is flat and is characteristic of the random background rate.

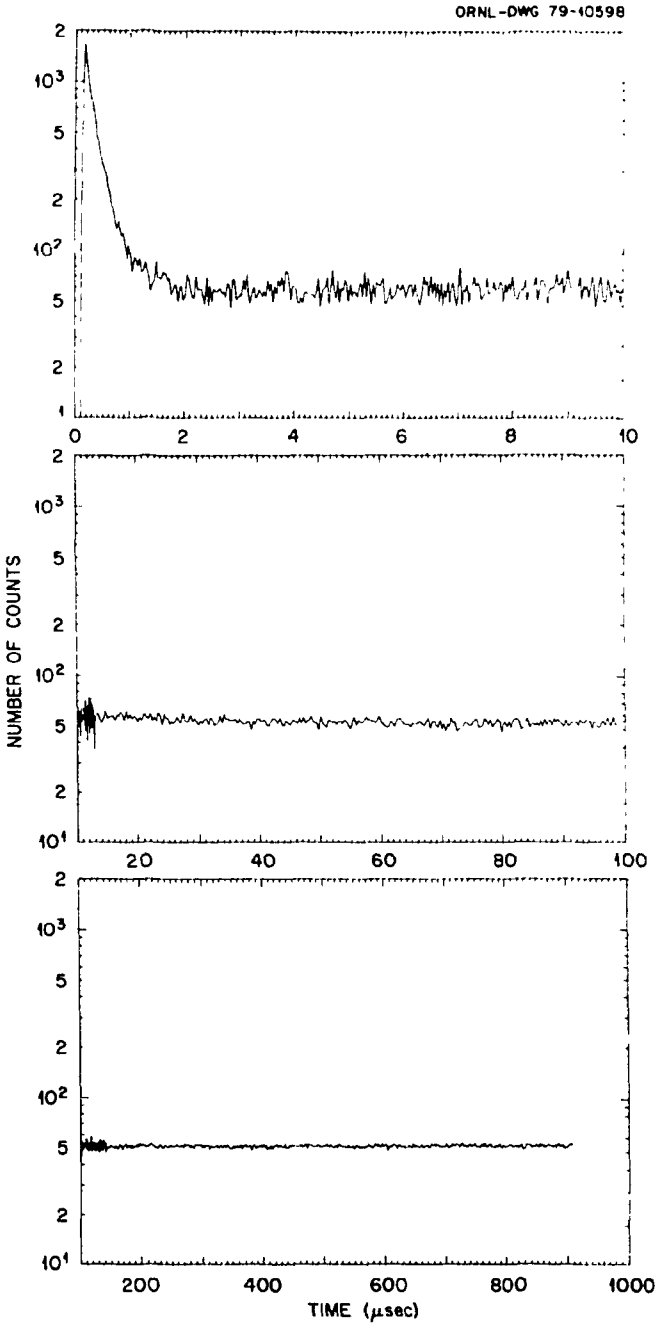

Fig. 21. Time distribution of tank events with a ∿ 950 disintegrations/sec ^{22}Na source at the tank center. Background was not subtracted. The early time structure has a ∿ 140 nsec decay period.

Table V-A shows that the resulting nubar data have a systematic increase of ~ 0.07 per 100 nsec of delay added. The invariant quantity R, shown in column 3 of Table V-A, is clearly sensitive to this trend also. Since k_3, k_{2B}, and k_{3B} contribute a negligible amount to the pile-up correction, a value of k_2 was sought which gave better agreement in the $\bar{\nu}$ and R values for the different values of τ. Table V-B shows the agreement obtained by decreasing k_2 by 9.5%, a change much greater than is implied by uncertainties in measuring τ, T, or the time of absorption integral. Accordingly, the pile-up correction previously calculated was reduced by the ratio of the weighted average of the $\bar{\nu}$ values in Table V-B to the τ = 95.3 nsec $\bar{\nu}$ value of Table V-A (0.99923). The uncertainty in the pile-up correction was then taken to correspond to the standard deviation of the four $\bar{\nu}$ values in Table V-B.

Correction for Absorption by the Photomultiplier and for the Off-Axis Position of the ^{252}Cf Source

In test runs following the tank efficiency calibration it was found that the photomultiplier tube and base of the proton-recoil detector caused a decrease in the observed $\bar{\nu}$ for ^{252}Cf. Several runs were made with the ^{252}Cf chamber in the experimental position (1/2 inch in from the thru-tube bottom and at the tank horizontal center) both with and without the photomultiplier assembly. This resulted in a correction factor of 1.00346 ± 0.00032 to be applied to the observed $\bar{\nu}$ of ^{252}Cf. This effect is primarily due to absorption by the boron in the glass P-M (13% B_2O_3 by weight). An additional correction factor of 1.00138 ± 0.00030 was found necessary to correct the observed $\bar{\nu}$ of ^{252}Cf to a position at the center of the tank and on the axis of the through tube. The origin of this latter effect is not presently understood, but it was verified to high precision through the use of a second, fixed ^{252}Cf

TABLE V-A. $\bar{\nu}$ vs. Deadtime

Deadtime (nsec)	Observed $\bar{\nu}$ Corrected for Pile-up	R
95.3 ± 1.2	3.11624 ± 0.00016	- 0.15368 ± 0.00007
197.6 ± 1.2	3.11844 ± 0.00028	- 0.15333 ± 0.00012
295.3 ± 1.2	3.12105 ± 0.00031	- 0.15293 ± 0.00013
396.5 ± 1.2	3.12322 ± 0.00031	- 0.15228 ± 0.00012

TABLE V-B. k_2 Reduced by 9.5%

Deadtime (nsec)	$\bar{\nu}$	R
95.3	3.11402	- 0.15395
197.6	3.11375	- 0.15392
295.3	3.11392	- 0.15386
396.5	3.11340	- 0.15361

chamber while mapping with the original chamber. The fixed chamber insured that drifts in the tank gain, etc. were not experienced. The horizontal position of the ^{252}Cf source was known to be within ± 0.2 cm of the tank center. From horizontal mapping, results shown in Fig. 22, it is concluded that this uncertainty leads to negligible error in nubar.

Uncertainty Due to the Fission Chamber Discrimination Level

The loss of recorded fission events below the finite discrimination level of the ion chamber could lead to error in the nubar determination through the known neutron number - fragment kinetic energy correlation or via the strong correlation in fragment and neutron directions. Thus loss of low kinetic energy fragments would tend to lower the observed nubar as would preferential loss of fragments traveling parallel to the chamber plates due to energy loss in the gold overcoating or imperfections in the source backing material. The directional effect would lead to no error for truly spherical symmetry of neutron detection. The variation of observed nubar was studied as a function of fragment pulse height by two parameter data acquisition. Integral results of the data for several bias (discrimination) levels are given in Fig. 23 along with a pulse height spectrum of the fission chamber in prompt coincidence with tank fission γ-rays for reference. It was inferred from the negligible change in $\bar{\nu}$ for biases in the low energy pulse height "valley" that the loss of events below the normal experimental bias (labelled 0 in Fig. 23) would lead to negligible error in the observed $\bar{\nu}$.

Correction for the "French Effect"

It has been suggested by Soleihac et al., as reported by Colvin[28] that the requirement of a fission chamber - tank coincidence to signal

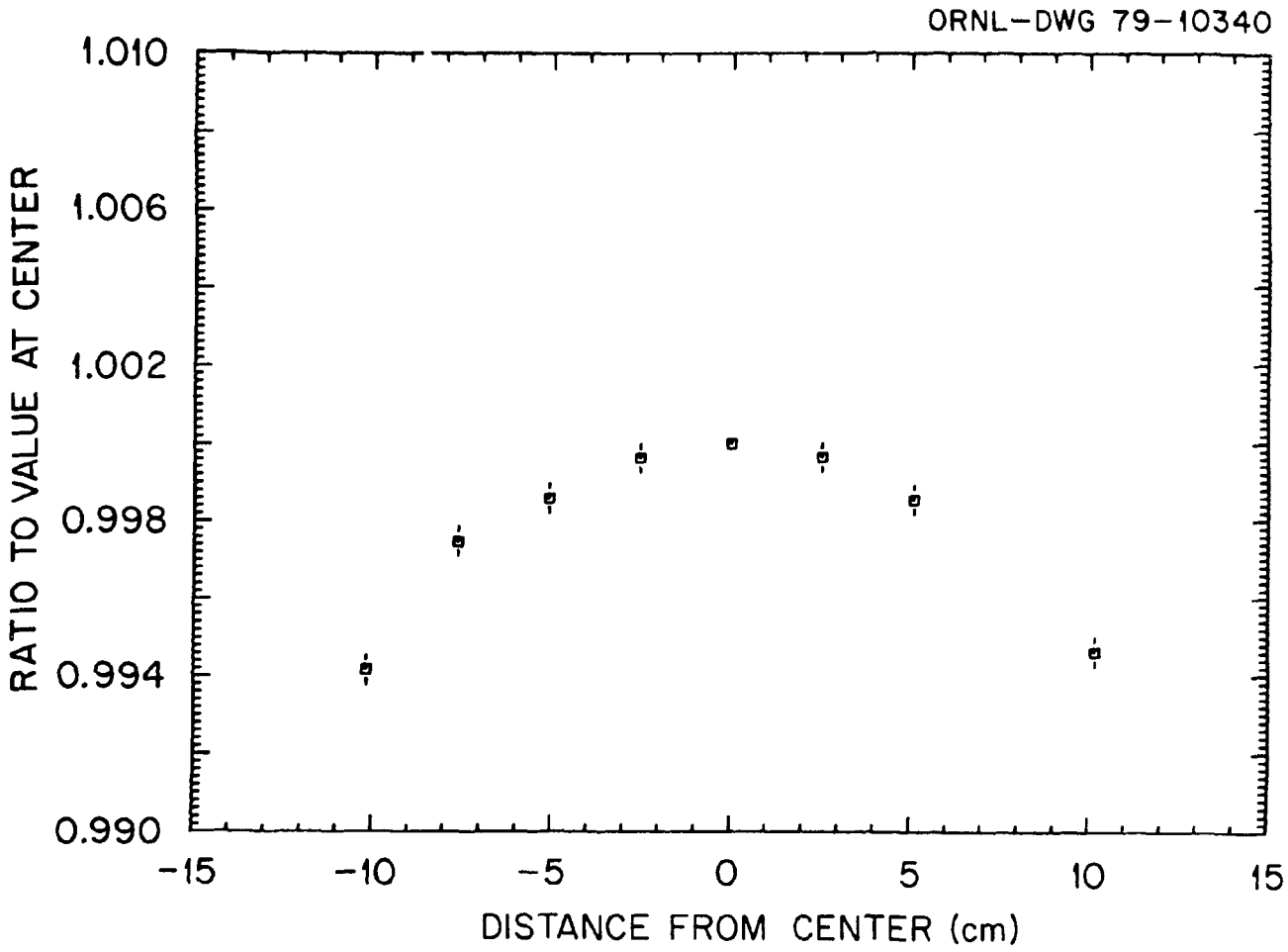

Fig. 22. Mapping of the tank response to ^{252}Cf neutrons as a function of source distance from the tank center along the through-tube center axis. The ordinate is the ratio of $\bar{\nu}$ at the source position to $\bar{\nu}$ for the source at the center of the tank.

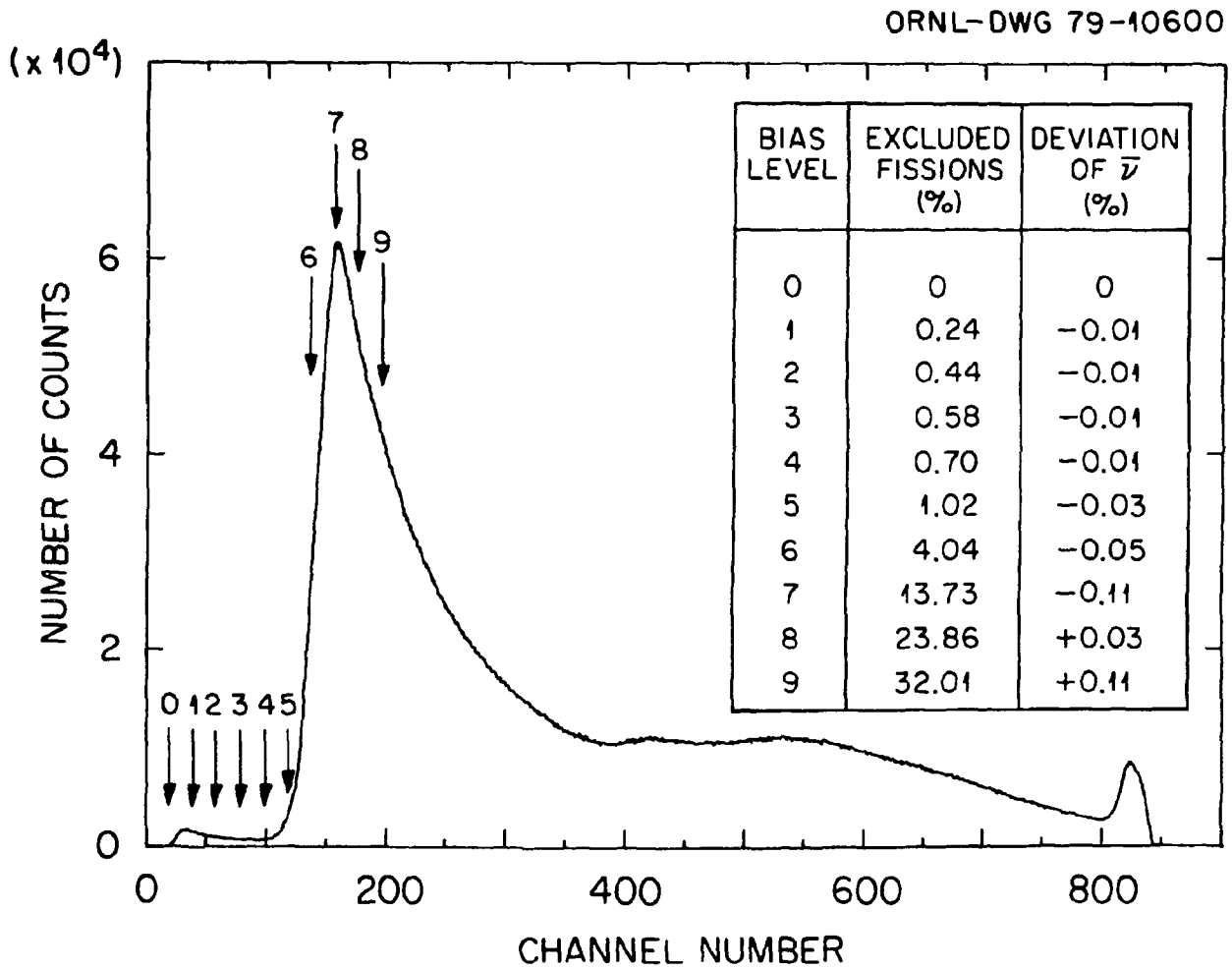

Fig. 23. Pulse height spectrum of ^{252}Cf chamber no. 7 in coincidence with prompt γ-rays from fission in the scintillator tank showing the percent deviation of observed nubar with chamber integral discimination level.

the fission event may bias the observed $\bar{\nu}$ to a higher value. A measurement of this effect was made. In order to accomplish this the fission chamber bias was raised to a level well above the alpha distribution (corresponding approximately to bias 2 in Fig. 23). Observed $\bar{\nu}$ was recorded separately for events both with and without a coincident tank pulse. After subtraction of background (and pile-up correction) the ratio of $\bar{\nu}$ for all events to that of coincidence events was 0.99970 ± 0.00013. This correction was made but with an assigned uncertainty equal to the correction since alpha pile-up cannot be totally eliminated as a contributing factor.

Correction for Delayed Gamma Rays

The observed value of nubar must be corrected for the detection of gamma rays emitted by isomers whose half-lives lead to a significant contribution in the time interval 0.5 - 50.5 μsec after fission, the neutron counting interval. This correction was calculated in the manner described by Boldeman.[3] The delayed gamma-ray yield data for the known isomers compiled in Ref. 3 were combined with the more recent data of Clark, Glendenin and Talbert[29] for the 0.16, 0.62, and 3.1 μsec isomers to give the values shown in Table VI. Following the suggestion of Ref. 3 the 26.7, 54.0, and 80 μsec isomer yields of Boldeman given in Table III of that reference were divided by the ratio of the Boldeman value for the 3.1 μsec isomer yield to the weighted average of all other measurements for that isomer. The resultant yield values for these longer half-life isomers are also given in Table VI-A, column 3. Column 4 of Table VI-A lists the estimated scintillator tank efficiencies above threshold for the isomer cascades and total cascade energies. Efficiencies were

derived by counting the tank fast discriminator response to a number of calibrated sources. These data, shown in Table VI-B, also demonstrate the gamma-ray energy equivalent corresponding to the tank threshold (∿ 900 - 975 keV). From the precursor yields, half-lives, and tank efficiencies, a correction of 0.010 in observed nubar ($\bar{n}$) was calculated with an estimated uncertainty of ± 25% of the correction.

Attempts were made to measure the delayed gamma-ray fraction directly through use of the "shape parameter,"

$$R = \frac{\sigma_\nu^2}{\bar{\nu}^2} - \frac{1}{\bar{\nu}} = \frac{\sigma_n^2}{\bar{n}^2} - \frac{1}{\bar{n}}$$

which is invariant with respect to changes in the neutron efficiency of the scintillator tank.[22,25] The invariance of R for the ORNL system is demonstrated in Fig. 24. The solid points in this illustration were obtained from the observed nubar data taken for a variety of tank neutron detection thresholds. Note that the prompt fission gamma-ray threshold was not varied, but remained at ∿ 930 keV. This was accomplished by bridging the tank fast pulses through a second constant fraction discriminator. Values of the efficiency were obtained from the observed nubar values by assuming $\bar{\nu}$ = 3.756. It can be seen that below about 82% neutron efficiency the value of R is indeed invariant to a high degree of precision. The "unstable" region above 82% has been suggested to be due to the effects of discriminator multiple-pulsing, after-pulsing of the phototubes or delayed gamma-rays.[30] The 82% level for the ORNL tank corresponds to approximately 2.1 MeV, which is just above the highest cascade energy given for the delayed gamma rays in Ref. 3. This also is near the energy of gamma rays from capture of neutrons in hydrogen, but since hydrogen

TABLE VI-A. Data for Delayed Gamma-Ray Correction

Half Life (μsec)	Total Cascade Energy (keV)	Yield per Fission (%)	Tank Efficiency (%)	Contribution per Fission
0.162	1692	1.04 ± 0.05	74	.0009
0.62	1505	0.28 ± 0.02	74	.0012
3.1	1891	0.54 ± 0.04	70	.0034
26.7	1710	0.34 ± 0.15	74	.0018
54.0	1110	0.45 ± 0.20	50	.0011
80	1710	0.58 ± 0.26	74	.0015
			Total Correction	.0099

TABLE VI-B. Radioactive Source Tank Calibration

Source	Total Energy (keV)	Tank Efficiency (%)
^{22}Na	2296	74 ± 3
^{207}Bi	88%: 1633 9%: 2339 3%: 569	69 ± 3
^{65}Zn	1115	56 ± 2
^{54}Mn	835	11.4 ± 0.4
^{137}Cs	662	0.90 ± 0.03

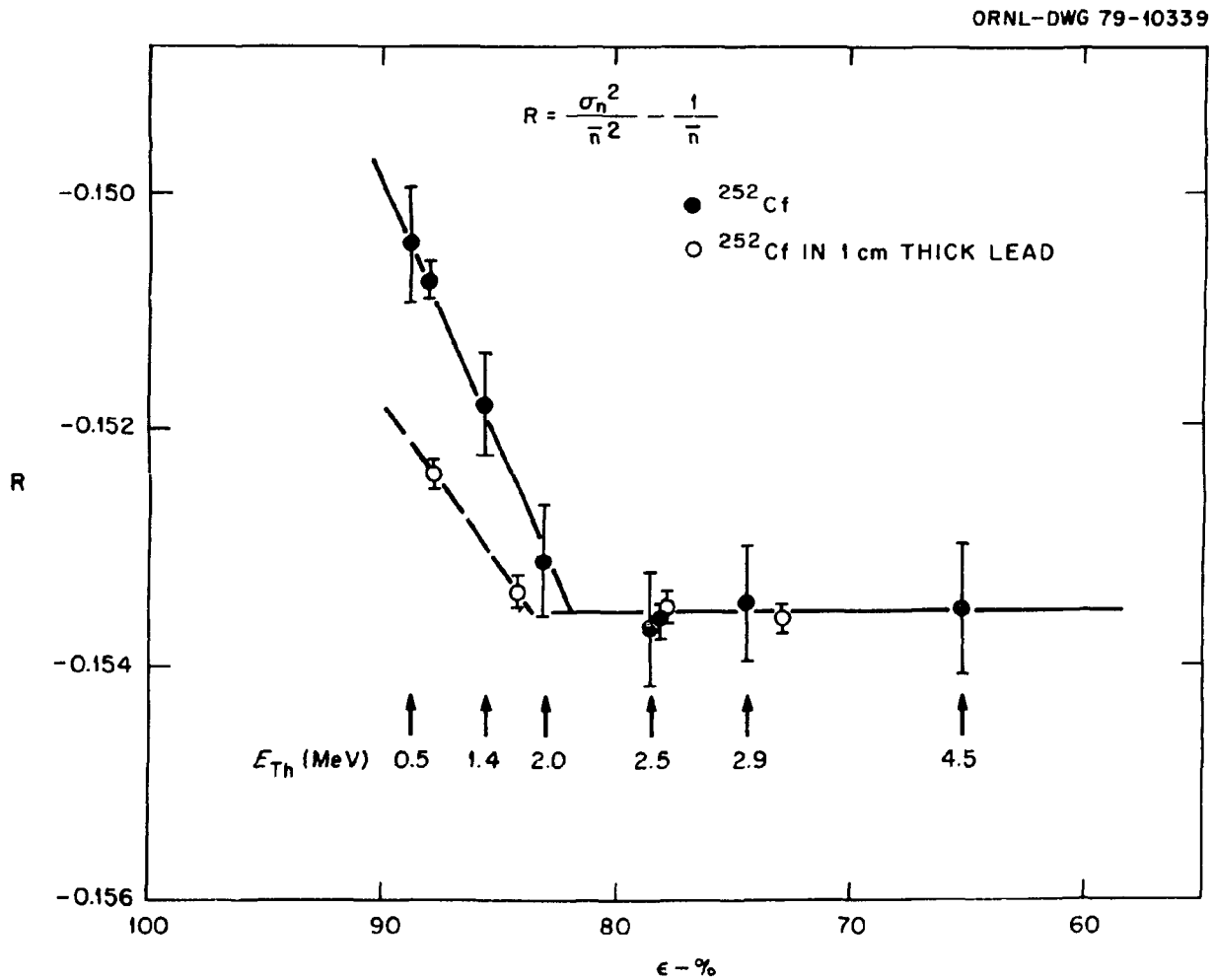

Fig. 24. Variation of the observed ^{252}Cf neutron number shape parameter, R, with tank neutron efficiency. The efficiency was varied by changing the tank pulse height discrimination level for neutrons, at a fixed level for fission gamma-ray response. The variation of R was observed with (open points) and without (solid points) a 1 cm thick lead pig around the ^{252}Cf chamber.

capture comprises part of the neutron efficiency, changes in detection of the hydrogen capture gamma ray should not affect the value of R. Furthermore, no evidence for after-pulsing has been observed with the ORNL scintillator system. As mentioned previously, the inversion of the proton-recoil data to zero's and one's only indicates negligible after-pulsing or discriminator multiple-pulsing for neutrons. Thus, it seemed reasonable to assume that the "unstable" region in R vs. ε is simply a result of delayed gamma rays. Measurements of R vs. ε were carried out with the ^{252}Cf fission chamber contained in a lead "pig" of 1 cm thickness. Since the prompt fission gamma rays would surely be perturbed, these experiments were done with the fission chamber biased just above the alphas and noise and with no tank prompt coincidence requirement. The results are shown as open points in Fig. 24. Although a significant change in $\bar{\nu}$ was recorded, it was determined by the measurements near 78% efficiency (with and without lead) that most of the effect in $\bar{\nu}$ was due to perturbation of the neutron efficiency of the tank by the 1 Kg lead pig. The value of R clearly is sensitive to the effect of lead in the region above 82% efficiency but shows no effect below 82%. The present absolute $\bar{\nu}$ measurement was carried out at $\sim$ 88% efficiency. Using the data with and without lead below 82% to calculate the perturbation of the neutron efficiency, it is possible to estimate the delayed gamma-ray fraction in the ^{252}Cf $\bar{\nu}$ experiment. The measurements were carried out a total of five times with slightly different geometry (lead pig on the through-tube bottom or on the center axis) and at least two different neutron detection thresholds. The net effect attributed to delayed gamma rays (average of five runs) was 0.0044 in nubar and the standard

deviation of the set was 0.0008. The "best" of this set of measurements is given in detail in Table VII. For this particular experiment, the primary californium source was placed on the axis of the tank through-tube and 3 cm to the forward of center. A second californium chamber was placed on the axis but 3 cm to the rear of center. The second source served as a fixed monitor for drifts, etc. Both low and high neutron detection threshold data were taken simultaneously for both detectors. The primary californium chamber was then removed, placed in the 1 cm thick lead pig and repositioned with the source 3 cm to forward of center and on the axis of the through-tube. The net effect which could be attributed to delayed gamma rays was 0.0047. A total error of ± 0.0021 was assigned to this value. If it is assumed that 60 ± 10% of the delayed gamma-ray effect on nubar is removed by the 1 cm thick lead, the total effect for $\bar{\nu} \sim 3.31$ is 0.0078 ± 0.0037 or 0.24 ± 0.11% of $\bar{\nu}$. The 60% absorption figure was estimated from measurements with sources. Approximately 40% of events from a ^{60}Co source, 65% from a ^{22}Na source and 70% from a ^{207}Bi source were removed by 1 cm of lead. The delayed gamma-ray fraction estimated in this way is in fair accord with the value, given earlier, that was calculated from the isomer half-lives and yield data.

Yet another approach may have some validity. One effect of adding delayed gamma rays to the neutron distribution is to lower the probability of observing zeros (or leave it unchanged) in addition to unpredictably altering the probabilities of higher orders of events. Thus, if it can be assumed that the high bias data (threshold $\geq$ 2 MeV) contain no delayed gamma rays and are representative of the "true" neutron distribution, relation (5) may be used to correct these data to a neutron efficiency

TABLE VII. Delayed Gamma Effect

	Cf #7		Monitor	
	$\bar{\nu}$	R	$\bar{\nu}$	R
		Low Bias		
#7 Bare	3.31531 ± 0.00039	-0.1507 ± 0.0002	3.31766 ± 0.00020	-0.1507 ± 0.0001
#7 in Lead Pig	3.30576 ± 0.00044	-0.1523 ± 0.0002	3.31840 ± 0.00022	-0.1507 ± 0.0001
Difference	0.00955 ± 0.00059		-0.00074 ± 0.00030	
		High Bias		
#7 Bare	3.11360 ± 0.00035	-0.1536 ± 0.0002	3.11604 ± 0.00017	-0.1536 ± 0.0001
#7 in Lead Pig	3.10874 ± 0.00043	-0.1539 ± 0.0002	3.11526 ± 0.00021	-0.1536 ± 0.0001
Difference	0.00486 ± 0.00055		0.00078 ± 0.00027	

Net Attributed to Delayed Gamma Rays: 0.0047 (= 0.00955 - 0.00486)
Estimated Systematic Error: 0.0015 (from the monitor)
Estimated Random Error: 0.0006

such that the corrected probability of zeros just equals that of the low bias data. The difference in the corrected high bias $\bar{\nu}$ and the observed low bias $\bar{\nu}$ should be just the minimum contribution of delayed gamma rays. This argument requires that the neutron efficiency, ε, is not correlated with the $P(\nu)$. This process was carried out on numerous runs where both a low and a high bias nubar were taken. The minimum delayed gamma ray effect at a $\bar{\nu} = 3.31$ appeared to be 0.014 to 0.016 or $\sim$ 0.45% of $\bar{\nu}$. This is somewhat higher than the two previous estimates. An attempt to establish an upper limit on the delayed gamma-ray yield was also attempted through use of the invariant parameter, R. If it is assumed that the delayed gamma rays are totally uncorrelated with the neutron number probabilities and only one isomer is formed in a fission event, an effect of $\sim$ 0.030 or 0.9% of $\bar{\nu}$ must be stripped out of the low bias distribution to change R from - 0.151 to the - 0.154 value of the "stable" region. This would appear to be almost the largest if not the maximum effect possible. Time of event distributions following ^{252}Cf fission indicate that at least the shorter half-life isomers are correlated with the number of neutrons detected and therefore 0.9% is undoubtedly an overestimate.

In view of the tenuous nature of both the data and deductions given above, it would seem most practical to follow precedent and accept the delayed gamma-ray fraction with expanded error, 0.30 ± 0.15% of $\bar{\nu}$, as calculated from the half-life and yield data of Table VI. This appears to be a reasonable compromise of the various estimates and has the advantage of putting the present correction on almost the same basis as for previous scintillator tank measurements.

Uncertainty Due to Monte Carlo Normalization

It seems reasonable that some error might result in the derived tank efficiency for ^{252}Cf neutrons which depends on the particular way chosen to normalize the Monte Carlo calculations. To this point the choices made in the analysis were to disregard the experimental data below 1.5 MeV, since the ^{10}B absorption and multiple scattering in the NE-213 increases toward lower neutron energies, and to treat all data energy groups together to derive a single normalization constant. This procedure tends to propagate errors in the shape of the cross sections used in the Monte Carlo analysis if the deviations are systematic. In order to reduce such effects, the Monte Carlo normalization was carried out in two additional ways. First, the experimental data above 1.5 MeV neutron energy were normalized for each energy bin separately. Energy groups below 1.5 MeV were normalized with the average factor (1.00233). This choice leads to a .08% higher $\bar{\nu}$ value, within the statistical error of the original analysis. As a second test, all energy groups from 0.50 ± .25 to 7.125 ± .375 MeV were individually normalized to the data. In this case the use of the low energy data is assumed to account for the ^{10}B absorption entirely and the observed $\bar{\nu}$ was not then corrected for this 0.35% effect. The resulting $\bar{\nu}$ was 0.24% higher than the original analysis.

For the synopsis of results given in Table VIII an effective tank efficiency was calculated corresponding to an average of the three normalization methods with an additional uncertainty included in quadrature corresponding to the standard deviation of the three values of $\bar{\nu}$ obtained.

TABLE VIII. Corrections and Estimated Uncertainties

Observed Value	$\bar{n}$ = 3.26369 ± 0.00029
Corrections	
Net Pile-up:	α_1 = 1.00715 ± 0.00027
Absorption in ^{10}B of Photo-tube:	α_2 = 1.00346 ± 0.00032
Off Axis Position of Fission Chamber:	α_3 = 1.00138 ± 0.0030
"French Effect"	α_4 = 0.99970 ± 0.00030
Delayed Gamma Rays:	γ = 0.010 ± 0.005
Tank Neutron Efficiency:	ε = 0.8703 ± 0.0019

$$\bar{\nu}_p(^{252}Cf) \cong (\bar{n}\cdot\alpha_1\cdot\alpha_2\cdot\alpha_3\cdot\alpha_4-\gamma)/\varepsilon$$
$$= 3.783 \pm 0.010$$

Uncertainty Due to "False Zeros"

False fission events with no associated neutrons could conceivably be initiated in the fission chamber by alpha particles and noise (particularly from the linac), thereby resulting in too low a value for $\bar{\nu}$. In the present experiment these effects were reduced to a negligible level through use of the tank fission gamma-ray coincidence requirement on fission events and by careful grounding of the fission chamber. "False zero" events in the proton-recoil detector can be initiated by noise, gamma rays, and charged particle reactions induced by beam neutrons in the material surrounding the NE-213 scintillator. The first two sources were reduced to a negligible level by the discrimination circuits. Fortunately only the (n,p) reactions contribute appreciably to the latter source, because the shorter range and nonlinear response in NE-213 of heavier charged particles discriminates strongly against false events from deuterons, alphas, etc. An estimate of the maximum effect of the (n,p) reactions was made using group cross sections for the materials involved (Si, Al, B, O, Na), the proton ranges, the hydrogen cross section, and the number of proton-recoils recorded for each incident neutron energy. This crude calculation indicated at most a 0.08% effect on the final $\bar{\nu}$ value. Since this is thought to be an overestimate, no correction was made; rather an uncertainty of this amount was included in quadrature in the efficiency calibration error.

Uncertainty Due to Uncertainty in the ^{252}Cf Neutron Spectrum

The ORNL scintillator tank is sufficiently large to be relatively insensitive to changes in the recommended ^{252}Cf neutron spectrum. The Monte Carlo calculations indicate a change of 0.004 in $\bar{\nu}$ for a 200 keV

increase in the Maxwellian average energy. One-half this amount was taken as an estimate of the error due to uncertainty in the fission neutron spectrum and was combined with the tank efficiency uncertainty.

XI. CONCLUSION

Table VIII summarizes the corrections and uncertainties that were applied to the present experiment. Table IX gives a neutron-number probability distribution derived from data taken with $\sim$ 2.5 MeV threshold on the scintillator tank neutron detection in order to reduce the effect of delayed gamma rays. The data were corrected to $\bar{\nu}$ = 3.78 using the efficiency inversion relation, Eq. (5), and therefore the distribution is subject to the assumption of no correlation between neutron efficiency and the P(ν). When adjusted to give the same assumed $\bar{\nu}$, this distribution is in good agreement with those reported by Boldeman[3] and by Ribrag et al.[25] using significantly smaller scintillator tanks, thus supporting the hypothesis of independence of ε_n and the P(ν).

Some additional sources of error in this type of measurement should be considered. Asplund-Nilsson et al.[2] have pointed out that both multiple scattering of the neutron in the proton recoil scintillator and escape of protons out of the scintillator lead to registration of the event at too high a neutron energy and a lack of knowledge as to the scattered neutron direction. The overall effect for their very small scintillator tank ($\sim$ 111 liters) appeared to be a small decrease in neutron efficiency toward low neutron energy. For the present measurement, the relative flatness of response of the scintillator tank with neutron energy and also with scattered neutron angle attained with the graphite plugs should reduce these effects to a negligible level. However, a future experiment

TABLE IX. The Neutron Number Distribution

ν	$P(\nu)$	Error[†]
0	0.00195	± 0.00017
1	0.02436	± 0.00073
2	0.12113	± 0.00141
3	0.27040	± 0.00116
4	0.30853	± 0.00081
5	0.18910	± 0.00124
6	0.06852	± 0.00073
7	0.01418	± 0.00022
8	0.00173	± 0.00005
9	0.00011	± 0.00001

$\bar{\nu}$ = 3.7827

$\sigma^2(\nu)$ = 1.5795

R = -0.15398 ± 0.00015

Total Fissions = 17,507,307

[†]The error analysis was provided by F. G. Perey.[31] See Appendix C for the correlation matrix.

incorporating two proton-recoil detector thicknesses is planned to quantify this further. Probably the most serious defect in the present experiment is the fall-off in neutron efficiency of the tank at very low neutron energies due to slow neutrons exceeding the time gate and to absorption of slow neutrons in the ^{10}B content of the photomultiplier. In future experiments this weakness will be largely eliminated through use of a smaller through-tube with a cadmium liner. At least one calibration experiment will be attempted with a solid-state type of proton-recoil detector in order to support the NE-213 results.

ACKNOWLEDGEMENTS

In addition to acknowledging the considerable benefit derived from the publications of previous experimenters, the authors would like to express their appreciation to the numerous staff members of the Oak Ridge National Laboratory who contributed both directly and indirectly to the execution of this project. Among those, special thanks go to Joe Pace and Noel Cramer for additional calculations of the scintillator tank absorption, to Temple Love and J. H. Todd for valuable help and discussion concerning the proper operation of the NE-213 proton-recoil detector, to Jack Craven who so rapidly adapted the SEL computer on-line analysis programs to the required 3-dimensional mode, and to R. W. Peelle and F. C. Maienschein for their continued encouragement and support. In addition, we greatly appreciated the many discussions and work of John Ullo at the Bettis Westinghouse laboratories who carried out a more detailed and independent Monte Carlo calculation of the tank neutron efficiency thereby greatly increasing confidence in our own result. The support of the ORELA operations group and craftsmen was greatly appreciated. Finally, the suggestions of Ben Diven of Los Alamos Scientific Laboratories in presentation of the results are gratefully acknowledged.

REFERENCES

1. J. C. Hopkins and B. C. Diven, Nucl. Phys., 48, 433 (1963).
2. I. Asplund-Nilsson, H. Conde, and N. Starfelt, Nucl. Sci. Eng., 16, 124 (1963).
3. J. W. Boldeman, Nucl. Sci. Eng., 55, 188 (1974).
4. D. W. Colvin, M. G. Sowerby, and R. I. MacDonald, Proc. IAEA Conf. Nuclear Data for Reactors, Vienna, I. 307 (1967).
5. A. De Volpi and K. G. Porges, Phys. Rev., C1, 683 (1970).
6. E. J. Axton, A. G. Bardell, and B. N. Andric, EANDC(UK)-110, p. 70, National Physical Laboratory (1969).
7. H. Bozorgmanesh, Thesis, U. of Michigan, 1977.
8. H. D. Lemmel, Conf. on Nuclear Cross Sections and Technology, Washington, D. C., NBS Special Publication 425, 1, 286 (1975).
9. J. W. Boldeman, International Specialists Symposium on Neutron Standards and Applications, National Bureau of Standards, NBS Special Publication 493, 182 (1977).
10. J. R. Smith, Seminar on Nuclear Data Problems for Thermal Reactor Applications, Brookhaven National Laboratory, EPRI NP-1098 (1979).
11. J. J. Ullo and M. Goldsmith, "Monte Carlo Analysis of Direct Measurements of the Thermal Eta (.025 eV) for ^{233}U and ^{235}U," WAPD-TM-1217, April (1975).
12. J. J. Ullo, (private communication).
13. J. J. Ullo, "A Monte Carlo Analysis of a Direct Measurement of the Average Neutron Yield from Spontaneous Fission of ^{252}Cf," WAPD-TM-1232, November (1976).

14. J. H. Marable and C. R. Weisbin, Advances in Reactor Physics, Proceedings of an ANS Topical Meeting, Gatlinburg, Tennessee, edited by E. G. Silver, 231 (1978), CONF-780401.

15. M. Becker, D. R. Harris, B. Quan, and J. M. Ryskamp, A Review of the Theory and Application of Sensitivity and Uncertainty Analysis, Proceedings of a Seminar-Workshop, Oak Ridge, Tennessee, 75 (1979), ORNL/RSIC-42.

16. The data acquisition programs were written by Jack Craven and Nancy Betz of the ORNL Computer Division (unpublished).

17. F. Gillespie, E. Kobisk, and coworkers of ORNL were responsible for the design and construction of the ion chamber.

18. H. L. Adair and P. R. Kuehn, Nucl. Instr. and Meth., 114, 327 (1974).

19. S. F. Mughabghab and D. I. Garber, Neutron Cross Sections, BNL-325, vol. 1, June (1973).

20. J. Harvey and G. Morgan (private communications).

21. J. Poitou and C. Signarbieux, Nucl. Instr. and Meth., 114, 113 (1974).

22. B. C. Diven, H. C. Martin, R. G. Taschek, and J. Terrell, Phys. Rev., 101, 1012 (1956).

23. J. Frehaut, Nucl. Instr. and Meth., 135, 511 (1976).

24. D. S. Mather, P. Fieldhouse, and A. Moat, Phys. Rev., 133, 1403 (1964)

25. M. Ribrag, J. Poitou, J. Matuszek, C. Signarbieux, Rev. Phys. Appl., 7, 197 (1972).

26. R. D. Hart, C. R. Cox, G. W. Dodson, M. Eckhause, J. R. Kane, M. S. Pandey, A. M. Rushton, R. T. Siegel, and R. E. Welsh, Phys. Rev. Lett. 39, 399 (1977).

27. J. C. Sens, Phys. Rev. 113, 679 (1959).

28. D. W. Colvin, Proc. 2nd Intern. Conf. Nuclear Data for Reactors, Helsinki, II, 195 (1970).

29. R. G. Clark, L. E. Glendenin, W. L. Talbert, Jr., Physics and Chemistry of Fission, Proceedings of the IAEA Symposium at Rochester, N.Y., Vol. II, 221 (1973).

30. C. Signarbieux, M. Ribrag, J. Poitou, and J. Matuszek, Nucl. Instr. and Meth., 95, 585 (1971).

31. F. G. Perey, private communication (June 1979).

APPENDIX A. ADDITIONAL TESTS

Since the writing of the main body of this report, several additional checks have been made with the tank $\bar{\nu}$ system. One test was designed to check for sensitivity to tank output pulse base line shifts due to prior pulses. An LED situated on top of the tank was pulsed at a steady rate of 1000 Hz at an amplitude which gave tank output pulses equivalent to $\sim$ 2.5 MeV. With the Cf No. 7 chamber in the through-tube at the tank center, the fission events which contained an LED pulse within the 50 μsec $\bar{\nu}$ gate were "tagged" and stored separately from fission events which were not followed by an LED pulse in the $\bar{\nu}$ counting gate. The pile-up corrected data are given below:

n	N'(n) Cf Only	Cf + LED	B'(n) Bkgd Only	Bkgd + LED
0	.0061	.0000	.9608	.0001
1	.0524	.0061	.0379	.9600
2	.1780	.0526	.0011	.0385
3	.2962	.1784	.0001	.0012
4	.2688	.2959	.0001	.0001
5	.1413	.2682		.0001
6	.0460	.1417		
7	.0097	.0460		
8	.0013	.0097		
9	.0002	.0013		
10	———	.0001	———	———
$\bar{n}$	3.434 ± .000	4.434 ± .001	0.041 ± .000	1.042 ± .000
Gates	21,120,085	1,198,493	18,038,967	1,021,161

The agreement in nubar of ^{252}Cf in the two cases (with and without the light pulse) constitutes a mild check of the stability of neutron sensitivity of the tank when more than one pulse occurs in the nubar gate and [illegible] of the pile-up correction procedure.

The observed nubar of ^{252}Cf was also studied for a rotation of the fission chamber. The normal position of the chamber was with the normal to the fission plates along the through-tube axis. Rotation of the chamber so that the normal was 60° to the through-tube axis resulted in an apparent decrease in nubar of 0.06 ± .01%. This effect was considered negligible for the present determination.

APPENDIX B. TANK NEUTRON EFFICIENCY CALIBRATION

AVERAGE SCATT. ANGLE (DEGREES)	EXPERIMENTAL EFFICIENCY	SCATT. ANGLE (DEGREES)	MONTE-CARLO EFFICIENCY†
	NEUTRON ENERGY 0.50+-0.25 MEV		
		7.5	.7767 ± .0034
		12.5	.8120 .0034
		17.5	.8419 .0033
		22.5	.8549 .0033
		27.5	.8609 .0033
		32.5	.8621 .0033
		37.5	.8641 .0033
		42.5	.8698 .0033
		47.5	.8675 .0033
52.51	.8662 ± .0019	52.5	.8700 .0033
57.65	.8638 .0013	57.5	.8740 .0033
62.5	.8602 .0013	62.5	.8769 .0033
66.93	.8562 .0013		
72.13	.8586 .0019	72.5	.8759 .0033
76.46	.8492 .0041		
	NEUTRON ENERGY 1.00+-0.25 MEV		
		7.5	.7493 .0034
		12.5	.8101 .0034
		17.5	.8470 .0033
		22.5	.8635 .0033
		27.5	.8643 .0033
33.94	.9144 .0271	32.5	.8736 .0033
38.3	.8728 .0030	37.5	.8752 .0033
42.51	.8738 .0018	42.5	.8759 .0033
47.32	.8738 .0013	47.5	.8864 .0033
52.32	.8726 .0015	52.5	.8824 .0033
57.21	.8727 .0019	57.5	.8801 .0033
62.31	.8726 .0023	62.5	.8866 .0033
67.2	.8755 .0029		
70.96	.8708 .0080	72.5	.8850 .0033
	NEUTRON ENERGY 1.50+-0.25 MEV		
		7.5	.7092 .0045
		12.5	.7900 .0040
		17.5	.8459 .0033
		22.5	.8673 .0033
29.8	.8856 .0308	27.5	.8757 .0033
33.27	.8716 .0036	32.5	.8732 .0034
37.35	.8758 .0018	37.5	.8760 .0033
42.43	.8774 .0017	42.5	.8819 .0033
47.62	.8801 .0023	47.5	.8827 .0032
52.4	.8814 .0027	52.5	.8872 .0032
57.6	.8806 .0026	57.5	.8867 .0033
62.37	.8785 .0032	62.5	.8889 .0033
66.26	.8725 .0069		
		72.5	.8936 .0033

AVERAGE SCATT. ANGLE (DEGREES)	EXPERIMENTAL EFFICIENCY		SCATT. ANGLE (DEGREES)	MONTE-CARLO EFFICIENCY†	
	NEUTRON ENERGY 2.00+-0.25 MEV				
			7.5	.6976 ±	.0046
			12.5	.7809	.0041
			17.5	.8414	.0037
			22.5	.8699	.0034
27.87	.8808 ±	.0216	27.5	.8711	.0034
32.38	.8756	.0028	32.5	.8809	.0033
37.41	.8781	.0028	37.5	.8835	.0032
42.57	.8825	.0026	42.5	.8849	.0032
47.72	.8866	.0031	47.5	.8868	.0032
52.64	.8852	.0032	52.5	.8900	.0032
57.25	.8884	.0033	57.5	.8934	.0031
61.64	.8889	.0051	62.5	.9018	.0030
			72.5	.8953	.0031
	NEUTRON ENERGY 2.50+-0.25 MEV				
			7.5	.6392	.0048
			12.5	.7479	.0035
			17.5	.8367	.0037
24.86	.8626	.0488	22.5	.8546	.0034
27.74	.8746	.0051	27.5	.8711	.0034
32.48	.8781	.0033	32.5	.8771	.0033
37.54	.8795	.0037	37.5	.8818	.0033
42.44	.8803	.0036	42.5	.8819	.0033
47.62	.8855	.0034	47.5	.8837	.0032
52.51	.8881	.0032	52.5	.8805	.0033
57.22	.8844	.0049	57.5	.8972	.0031
60.6	.8810	.0114	62.5	.8909	.0032
			72.5	.8925	.0031
	NEUTRON ENERGY 3.00+-0.25 MEV				
			7.5	.5797	.0049
			12.5	.7330	.0044
			17.5	.8207	.0038
24.35	.871	.0068	22.5	.8510	.0036
28.63	.8736	.0045	27.5	.8632	.0035
33.35	.8738	.0039	32.5	.8779	.0033
37.78	.8789	.0036	37.5	.8820	.0033
42.48	.8819	.0036	42.5	.8853	.0032
47.45	.8844	.0035	47.5	.8893	.0032
52.14	.8859	.0042	52.5	.8921	.0031
56.71	.8859	.0073	57.5	.8952	.0031
			62.5	.8972	.0030
			72.5	.8973	.0030

AVERAGE SCATT. ANGLE (DEGREES)	EXPERIMENTAL EFFICIENCY		SCATT. ANGLE (DEGREES)	MØNTE-CARLØ EFFICIENCY†	
	NEUTRØN ENERGY 3.50+-0.25 MEV				
			7.5	.6784 ±	.0047
			12.5	.7423	.0044
			17.5	.8263	.0038
23.04	.8524 ±	.0091	22.5	.8562	.0035
27.86	.8752	.0052	27.5	.8676	.0034
32.75	.8749	.0046	32.5	.8722	.0034
37.51	.8816	.0041	37.5	.8767	.0033
42.5	.8798	.0038	42.5	.8821	.0033
47.44	.8833	.0046	47.5	.8890	.0032
52.07	.8931	.0056	52.5	.8851	.0032
55.89	.8883	.0149	57.5	.8861	.0032
			62.5	.8877	.0032
			72.5	.8994	.0030
	NEUTRØN ENERGY 4.00+-0.25 MEV				
			7.5	.6289	.0048
			12.5	.7149	.0037
			17.5	.8137	.0039
21.99	.8582	.0094	22.5	.8417	.0037
27.72	.8699	.0048	27.5	.8574	.0035
32.45	.8697	.0043	32.5	.8713	.0034
37.82	.8762	.0041	37.5	.8762	.0033
42.55	.8826	.0046	42.5	.8818	.0033
47.02	.8860	.0051	47.5	.8883	.0032
51.74	.8866	.0080	52.5	.8842	.0032
55.33	.8752	.0355	57.5	.8871	.0032
			62.5	.8911	.0032
			72.5	.8933	.0031
	NEUTRØN ENERGY 4.50+-0.25 MEV				
			7.5	.5917	.0049
			12.5	.6904	.0046
			17.5	.8031	.0040
			22.5	.8463	.0036
26.91	.8596	.0044	27.5	.8520	.0036
32.33	.8656	.0045	32.5	.8641	.0035
37.06	.8694	.0047	37.5	.8686	.0034
42.2	.8762	.0048	42.5	.8811	.0033
47.2	.8698	.0075	47.5	.8799	.0033
51.22	.8876	.0108	52.5	.8824	.0033
			57.5	.8832	.0032
			62.5	.8822	.0032
			72.5	.8899	.0031

ANGLE OF SCATT. ANGLE (DEGREES)	EXPERIMENTAL EFFICIENCY		SCATT. ANGLE (DEGREES)	MONTE-CARLO EFFICIENCY†	
			NEUTRON ENERGY 5.00+-0.25 MEV		
			7.5	.5064	.0038
			12.5	.6505	.0038
			17.5	.7657	.0038
24.73	.824	.0097	22.5	.8249	.0038
27.14	.8414	.0046	27.5	.8396	.0037
32.56	.8526	.0054	32.5	.8524	.0036
37.25	.8627	.0059	37.5	.8618	.0035
42.2	.8659	.0072	42.5	.8700	.0034
46.76	.8754	.0082	47.5	.8725	.0034
51.16	.8682	.0136	52.5	.8780	.0033
			57.5	.8816	.0033
			62.5	.8826	.0032
			72.5	.8849	.0032
			NEUTRON ENERGY 5.625+-0.375 MEV		
23.88	.8205	.0051	22.5	.8059	.0040
27.95	.8400	.0058	27.5	.8329	.0038
32.4	.8535	.0045	32.5	.8455	.0036
37.34	.8534	.0051	37.5	.8552	.0035
42.09	.8606	.0064	42.5	.8635	.0035
46.82	.8636	.0091	47.5	.8661	.0034
			NEUTRON ENERGY 6.375+-0.375 MEV		
22.51	.8179	.0055	22.5	.7854	.0041
27.11	.8251	.0050	27.5	.8177	.0039
32.35	.8386	.0063	32.5	.8314	.0038
37.45	.8400	.0072	37.5	.8420	.0037
42.07	.8575	.0092	42.5	.8501	.0036
46.12	.8349	.0226	47.5	.8568	.0035
			NEUTRON ENERGY 7.125+-0.375 MEV		
22.47	.7795	.0059	22.5	.7702	.0042
27.84	.8284	.0083	27.5	.8000	.0040
32.48	.8211	.0070	32.5	.815	.0039
37.89	.8302	.0089	37.5	.8267	.0038
42.35	.8335	.0099	42.5	.8360	.0037
46.06	.8627	.0241	47.5	.8442	.0037

†These efficiencies have all been multiplied by the normalization factor 1.00233.

APPENDIX C

The error analysis for the P(ν) distribution contained the statistical uncertainties, an estimated ± 3.8% uncertainty in the pileup parameter (k_2 = 0.004851), and an estimated ± 0.22% uncertainty in the detector efficiency (ε = 0.7738 based on a ν of 3.783). Under these assumptions the following elements of the P(ν) correlation matrix (multiplied by 100) were derived:[1]

	P_0	P_1	P_2	P_3	P_4	P_5	P_6	P_7	P_8	P_9
P_0	100									
P_1	-48	100								
P_2	- 7	85	100							
P_3	-16	88	84	100						
P_4	-46	-34	-55	-67	100					
P_5	-23	-67	-87	-75	60	100				
P_6	-14	-72	-88	-83	74	83	100			
P_7	- 8	-68	-81	-75	58	85	71	100		
P_8	- 2	-44	-51	-48	38	49	58	19	100	
P_9	0	-13	-15	-14	11	16	13	27	-41	100